Since January 2020 Elsevier has created a COVID-19 resource centre with free information in English and Mandarin on the novel coronavirus COVID-19. The COVID-19 resource centre is hosted on Elsevier Connect, the company's public news and information website.

Chemical Engineering Journal 452 (2023) 138894

Contents lists available at ScienceDirect

Chemical Engineering Journal

journal homepage: www.elsevier.com/locate/cej

Review

Modulation of Z-scheme photocatalysts for pharmaceuticals remediation and pathogen inactivation: Design devotion, concept examination, and developments

Mope Edwin Malefane *, Potlako John Mafa, Thabo Thokozani Innocent Nkambule, Muthumuni Elizabeth Managa, Alex Tawanda Kuvarega *

Institute for Nanotechnology and Water Sustainability, College of Science, Engineering and Technology, University of South Africa, Florida 1709, Johannesburg, South Africa

ARTICLE INFO

Keywords:
Interfacial charge-transfer
Pharmaceutical degradation
Solar energy harvesting
Viral and bacterial inactivation
Z-scheme heterojunctions

ABSTRACT

The recent outbreak of Covid-19 guarantees overconsumption of different drugs as a necessity to reduce the symptoms caused by this pandemic. This triggers the proliferation of pharmaceuticals into drinking water systems. Is there any hope for access to safe drinking water? Photocatalytic degradation using artificial Z-scheme photocatalysts that has been employed for over a decade conveys a prospect for sustainable clean water supply. It is compelling to comprehensively summarise the state-of-the-art effects of Z-scheme photocatalytic systems towards the removal of pharmaceuticals in water. The principle of Z-scheme and the techniques used to validate the Z-scheme interfacial charge transfer are explored in detail. The application of the Z-scheme photocatalysts towards the degradation of antibiotics, NSAIDs, and bacterial/viral inactivation is deliberated. Conclusions and stimulating standpoints on the challenges of this emergent research direction are presented. The insights and up-to-date information will prompt the up-scaling of Z- scheme photocatalytic systems for commercialization.

1. Introduction

A consensus has been reached by different stakeholders that energy crisis and environmental pollution are primary challenges facing the world in the 21st century with water pollution considered as the major contributor of human adverse health effects and environmental deterioration. Water pollutants consist of heavy metals, pharmaceuticals, bacteria, and organic matter from domestic waste. It is estimated that water pathogens such as bacteria, viruses, fungi, protozoa, prions and parasites initiates about 80 % of ailments in unindustrialized nations [1] and there is poor prophylaxis of waterborne epidemics globally [2]. Pharmaceuticals form a major constituent of priority pollutants in aquatic environments initiating frequent detection studies and possible remediation techniques being a substance of contemporary attention.

Photocatalysis is defined as a technique that results in production of oxidizing agents like hydroxyl radicals ($^{\bullet}OH$), superoxide anion radical ($^{\bullet}O_2^-$), holes (h^+), and singlet oxygen ($^1O_2$). In semiconductor photocatalysis, the initial step (step i) involves the absorption of light energy equal or greater than the bandgap of the semiconductor. The subsequent steps that follow photoexcited electrons and holes may take four pathways that are distinctively known as electrons and holes surface recombination (route A), electrons and holes bulk recombination (route B), surface oxidation reaction initiated by photoexcited holes (route C), and surface reduction initiated by photoexcited electrons (route D) [3,4]. Routes A and B occur within a period of a few ps - ns [5]. The photodegradation activity of photocatalysts reliant on these four routes is determined by (1) the light harvesting ability with a requirement of wide light energy absorption range, (2) rapid migration of photogenerated charges and transportation to the surface of the semiconductor active/reaction site, and (3) strong reduction and oxidation reactions at the photocatalytic reaction sites [6]. However, the requirement of wide light energy absorption is a narrow bandgap energy of the photocatalyst as the Coulomb field equation, i.e., $F_c = Kq_eq_h/r^2$ demonstrates that force (F_c) of attraction of photogenerated charge pairs (q_e, q_h) is inversely proportional to the reduction in bandgap energy (r) [7], K is proportionality constant. Ironically, a wide bandgap results in strong redox ability and less likeliness for recombination of excited electrons and holes, creating a challenge for a distinct semiconductor to

* Corresponding authors.
E-mail addresses: mopemalefane@gmail.com (M. Edwin Malefane), kuvarat@unisa.ac.za (A. Tawanda Kuvarega).

https://doi.org/10.1016/j.cej.2022.138894
Received 9 June 2022; Received in revised form 8 August 2022; Accepted 25 August 2022
Available online 29 August 2022

possess all features that are significant for proficient photocatalytic reactions [8].

Diverse tactics investigated for possible improvement of the general efficiency of semiconductors for removal of pharmaceuticals include metal doping [9], non-metal doping [10], multi-elemental doping with metals and/or non-metals [11], use of supports [12], and formation of heterojunctions [13,14]. The contribution of heterojunctions towards abatement of different classes of pharmaceuticals such as β- blockers, hormones, antibiotics, cholesterol-lowering drugs, oestrogens, antipsychotics, non-steroidal anti-inflammatory drugs (NSAIDs) and analgesics has been studied recently [15–20]. There are numerous heterojunctions that have been reported in literature for effective degradation of pollutants and they comprise p-n, traditional type II, R-scheme, C-scheme, p-*n*-p and Z-scheme heterojunctions, etc. [21–24]. The Z-scheme heterojunction evolved from mimicking the natural photosynthesis process that plants employ for food generation [25]. The illustration of electron transfer process in natural photosynthesis forms a shape identical to the English letter "Z" initiating its name. In some recent reviews, the natural photosynthesis process has been described in detail for better understanding [25–27]. In summary, Z-scheme photosynthesis encompass garnering of solar energy through chlorophylls and their subsequent transfer to the reaction centre to initiate water oxidation on the donor side of photoreaction system II (PS II) while nicotinamide adenine dinucleotide phosphate (NADP) aided reduction of CO_2 to carbohydrates occurs at the acceptor side of photoreaction system I (PS 1) [25]. Like photosynthesis, Z-scheme photocatalytic heterojunctions offers high charge separation quantum efficiency with presence of PS I and PS II promising to conquer inadequacies of strong redox ability and wide light absorption requirements.

Comprehensive explorations directed at mirroring the natural photosynthesis process resulted in numerous Z-scheme discoveries that are generally classified as liquid phase (redox mediator/traditional), all solid state (indirect), direct (Step-scheme) and/or dual Z-scheme photocatalytic systems. In traditional or liquid phase Z-scheme which was the first to be explored, the use of electron mediators facilitates migration of electrons and is applicable only to liquid samples [28]. Electron acceptors attract and transfer electrons from one semiconductor to another while electron donors fill the holes on the other semiconductor under irradiation by light energy [28]. Indirect Z-scheme uses solid electron mediators as a means to transfer electrons from one semiconductor to another after light irradiation [29], while direct Z-scheme normally employs direct semiconductors contact to circumvent the use of mediators under light irradiation [30]. Certain approaches that are used to fabricate direct Z-scheme composites were ascertained to guide the geometry of the Z-scheme mechanism and the general geometrical patterns can be classified into surface-decorated systems, Janus-type systems, and core–shell architectures as reported by Xu et al. [6]. The surface decorated geometry in Z-scheme entail the deposition of one photocatalyst on the surface of another with irregular or regular distributions. Janus-type systems possess a stack of one semiconductor on top of another while core–shell architectures means one semiconductor forms a core of another. In dual Z-scheme heterostructure, three semiconductors are oriented in a cascade, arrow up or arrow down classification based on their pattern shape such that one semiconductor is an electron mediator, a reduction semiconductor, or an oxidative semiconductor, respectively [31]. Generally, achieving high quantum efficiency with Z-scheme mechanisms requires proper selection of semiconductors such that one semiconductor is accountable for high reduction performance and stability while the other provides high oxidation stability and performance under light irradiation. The urgency in development of Z-scheme photocatalytic systems ensured an exponential increase of their uses in different applications. The design of Z-scheme photocatalytic systems is governed by proper band alignment and work functions of the distinctive semiconductors, availability of charge transportation path, and materials property manipulations such as defects generation.

Numerous reviews have been compiled on the topic of different properties and applications of Z-scheme photocatalytic systems [3,6,32]. Xue et al. emphasized elementary ideologies and construction of silver-based Z-scheme photocatalytic systems with clear role of metallic silver explored under numerous applications [33]. Wang et al. [27] systematically outlined different and recent redox mediated properties and applications of traditional Z-scheme photocatalytic systems for water splitting towards renewable H_2 evolution focusing on reaction mechanisms and different performance of various elected acceptor and donor pairs. Important discussions exists to distinguish the different charge transfer mechanisms involved in type II, Z-scheme and Step-Scheme mechanisms with the aim of signalling misinterpretations that may stir up [34]. Charge transfer mechanisms of direct Z-scheme have been analysed to occur through internal electric field (IEF), interfacial defect states and selective facet manipulation [35]. However, no specific review channels its discussion to pharmaceuticals which, considering the current Covid-19 pandemic outbreak, is of urgent attention due to an upsurge of drugs usage. It is imperative to outline appropriate designs, analyse the concept of Z-scheme towards degradation of pharmaceuticals, and the possibility of employing Z-scheme photocatalytic systems for removal of pathogens and antibiotics that are employed to reduce the impact of Covid-19.

This review focusses on the applications of Z-scheme composites towards degradation of pharmaceuticals (NSAIDs, antibiotics) and antimicrobial activity, the principles and concept proof of Z-scheme mechanism and efficiency, respectively. Moreover, the applications of Z-scheme photocatalysts for potential laboratory scale wastewater treatment plants and their real industrial applications towards mineralization of pollutants and medical applications have been reviewed. Lastly, suggestions on future directions and recommendations are made towards realization of industrial applications of Z-scheme heterojunctions.

2. Principle of Z-scheme

Z-scheme heterojunction can be described as a type of heterojunction that comprises distinct reduction and oxidation centres from two or more semiconductors forming two distinctive systems (PS I and PS II) after initial absorption of light energy equal or greater than their respective bandgap energies with or without the aid of electron mediators. The evolution of Z-scheme mechanism follows scientific studies and understanding of the natural photosynthesis and it has garnered enormous attention as the possible solution for the current water deterioration catastrophe and the energy calamity.

The key experiment towards Z-scheme concept was the two light reaction two-pigment system in 1957 known as the Emerson enhancement effect in oxygenic photosynthesis which showed two distinctive reaction sites of chlorophyll *a* and chlorophyll *b* for long-wave system and other reactions, respectively. The natural photosynthesis Z-scheme mechanism was first proposed by Hill and Bendall in 1960 despite not mentioning the important discovery of Emerson in their theoretical analysis and subsequent studies were conducted by other researchers to enhance the understanding of the mechanism involved during conversion of water and carbon dioxide into carbohydrates [36,37]. The Z-scheme photosynthesis process is summarised in Fig. 1a. Natural Z-scheme photosynthesis entails the generation of sugars through redox reactions that occur at two distinctive reduction and oxidation centre chlorophylls in photosystem II (PS II) and photosystem I (PS I), respectively. PS II chlorophylls absorb photons ($\lambda \leq 680$ nm) for generation of electron and hole pairs, with the holes oxidising water into oxygen, protons which converts ADP (adenosine diphosphate) into ATP (adenosine triphosphate), and electrons (transferred along the electron transport chain to quench holes generated in PS I) [27]. The transfer of electrons between the two photosystems involved in a Z-scheme photosynthesis is spontaneous. PS I absorbs photons ($\lambda \leq 700$ nm) to generate photoexcited electrons and holes, and the quenching of the holes elongates the lifespan of the electrons in PS I for reduction of

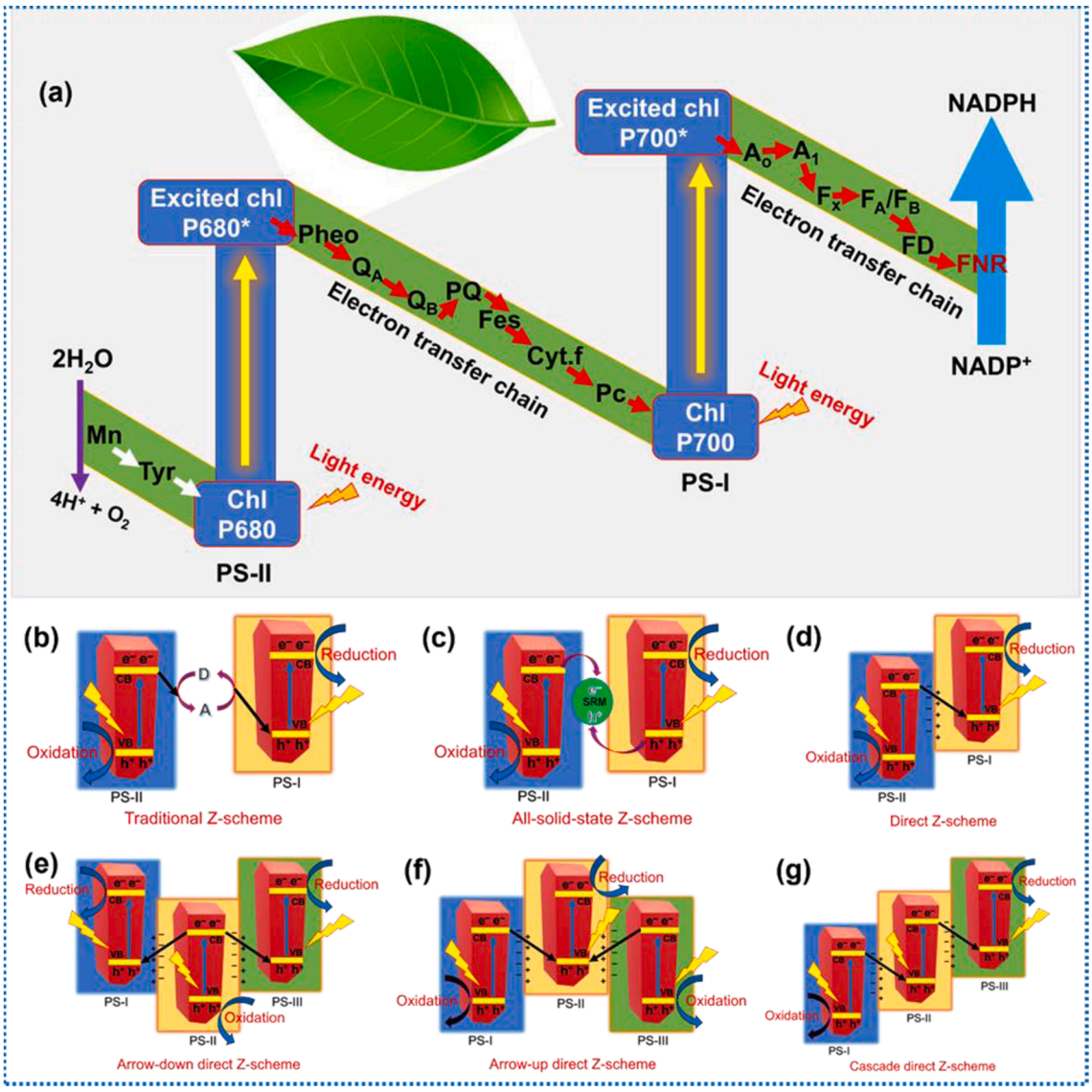

Fig. 1. Illustration of (a) Z-scheme photosynthesis, (b) traditional Z-scheme, (c) Indirect Z-scheme, (d) Direct Z-scheme, and (e) arrow-down dual, (f) arrow-up dual, and (g) cascade dual types Z-scheme.

NADP+(nicotinamide adenine dinucleotide phosphate) to NADPH [27]. Eventually, it was approved that the photosynthesis of plants employs a Z-scheme mechanism. Later in 1979, the first artificial Z-scheme photocatalysts was theoretically proposed by Bard [7] which included the linking of two photocatalytic systems with electron mediators of redox ion pairs. This was regarded as the first generation of Z-scheme called the traditional Z-scheme photocatalyst or a liquid-phase Z-scheme. It constitutes of two semiconductors with a dissolved redox intermediary comprising of an electron acceptor/donor pair. After illumination by light irradiation, the reductive and oxidative semiconductors produce electrons and holes such that electrons in conduction band of oxidative semiconductor react with the electron acceptor generating electron donor while the holes accumulating on the valence band of the reductive semiconductor reacts with the electron donor to generate an electron acceptor (Fig. 1b). The highly reductive electrons and oxidative holes in the conduction band and valence band of reductive semiconductor and oxidative semiconductor are tailored for initiation of photocatalytic reaction and to sustain the optimization of the systems redox potential [38].

Initially, the redox mediator that was first demonstrated in 2001 by Abe et al. was an IO_3^-/I^- shuttle redox mediator pair for water splitting. Comparisons of other redox mediators (I_3^-/I^- with IO_3^-/I^-, Fe^{3+}/Fe^{2+}, $[Co(bpy)_3]^{3+/2+}$ and $[Co(phen)_3]^{3+/2+}$) and their exploration followed the enhancement of the performance of the traditional Z-scheme heterostructures by different groups for successful transportation of photoexcited electrons from the conduction band of oxidative semiconductor (PS I) to the valence band of reductive semiconductor (PS II) [39]. Ideally, all applications conducted with traditional Z-scheme photocatalysts were limited to liquid media (such as water splitting) as the redox mediator should be dissolved for optimum performance. Other limitations to the practical exploitation of liquid-phase Z-scheme photocatalytic composites include the suppression of photocatalytic performance that can be initiated by possibility of backward reactions induced by competition of pollutant redox reactions between semiconductors and redox mediators. Moreover, pH sensitivity, competition of light absorption between catalyst and coloured redox mediators pairs like Fe^{3+}/Fe^{2+}, and slow charge carriers transportation due to hindrance by diffusion of redox ion pairs adds to the limiting factors of traditional Z-scheme system [6]. More detailed description of the limitations of Liquid-phase Z-scheme mechanism was described in a review by Xu et al. [34].

The inexorable limitations of the applicability of the traditional Z-

scheme was not adequate to halt explorations of this system, however, further research was tailored to address these limitations and broaden the applicability scope to include other environmental samples. This later resulted in unearthing the second generation of Z-scheme photocatalysts proposed by Tada et al. in 2006 and it was named all solid state Z-scheme mechanism [40]. The improvement of all solid state/indirect Z-scheme system compared to traditional Z-scheme was that instead of dissolved redox pairs, solid electron mediators were used as shuttles for photo-excited electrons from conduction band of oxidative semiconductor to the valence band of reductive semiconductor. The pioneering work was that of Tada and co-workers in 2006 involving a noble metal Au as electron shuttle between oxidative TiO_2 and reductive CdS [40]. In all solid state/indirect Z-scheme photocatalysis, both oxidative and reductive semiconductors are illuminated with light irradiation to generate respective excited electrons and holes pairs (Fig. 1c). The solid redox mediator (SRM) then shuttles the electrons from the conduction band of the oxidative semiconductor into the valence band of the reductive semiconductor to combine with holes. Ideally, separation of photogenerated electrons and holes will be achieved, and improved photocatalytic reaction activities will be realised with improved scope of applicability. The employed SRMs are noble metals (gold, silver, bismuth, etc.) [41], carbon based materials (exfoliated graphite, graphene, etc.) [42], and other metal oxide semiconductors (e.g. SrO) [43].

Despite successful fabrication of indirect Z-scheme, it still suffers some drawbacks as the conductors/mediators reported in literature are all visible light active and can result in light absorption competition with the semiconductors, reducing light harvesting activity, and in turn lowering photocatalytic efficiency. When noble metals are used, the cost of the overall photocatalyst hinders the large-scale applicability of this generation of Z-scheme photocatalysts while there is not enough literature to support the activity of alkali earth metal oxides use as electron shuttles, with lack of experimental evidence. The use of noble metals may also generate Schottky barriers that may hinder transfer of electrons from conduction band of either reductive or oxidative semiconductor as explicitly described elsewhere [34]. Lastly, it is difficult, from materials perspective, to ensure that conductors or solid electron mediators loaded on the catalysts surfaces lie between the two semiconductors such that they will act as electron shuttles [34]. While there are obvious challenges associated with traditional and all solid state Z-scheme systems, their photocatalytic activity still has high conversion quantum efficiency due to isolated centres for performance of redox reactions compared to other heterojunctions like type II or p-n heterojunctions that sacrifice the redox power for sufficient charge separation.

The necessity to address shortcomings of all solid state Z-schemes and improve the substantial capability of charge separation in Z-scheme photocatalytic composites towards robust and more stable pollutant degradation gave rise to the third generation of Z-scheme systems that was understood in 2009 and named the direct Z-scheme mechanism by Wang et al. through the fabrication of CdS/ZnO by wet-chemistry method for hydrogen evolution reaction under simulated solar light irradiation with 1805 $\mu mol\ h^{-1}g^{-1}$ [44]. The direct Z-scheme generation does not need the use of mediators like redox pairs or conductors like traditional and indirect Z-scheme systems, respectively [45–48]. The problems associated with electron mediators such as shielding effect, backward reaction, and photo-corrosion are overcame by formation of a direct surface contact between semiconductors shortening the electron transfer path [28]. In a direct Z-scheme system, the semiconductors are bombarded with radiation energy equal or greater than their respective band gaps to generate photoexcited electrons and holes respectively (Fig. 1d). The generation of electron hole pairs requires an oxidative semiconductor and a reductive semiconductor like in other generations of Z-scheme photocatalysts such that electrons in the conduction band (CB) of the oxidative catalyst neutralizes the holes in the valence band of the reductive semiconductor to enhance the reduction and oxidation capability of the oxidative and reductive semiconductors respectively [41,48,49]. The potential level of PS II lies at a potential energy less than the potential energy position of the VB of PS I and potential energy of PS I CB should be greater than the potential energy of PS II CB [28,50]. This will ensure that after equilibrium, electrons will easily migrate from the conduction band of PS II under induced electric field to the valence band of PS I [28]. In this system, since no mediators are required, direct contact between semiconductors have been envisaged to initiate this charge transfer mechanism since it was reported in 2009 [51]. The other reported aspects that enhances the direction of the charge flow in Z-scheme photocatalysis is the build in electric field [28] while band edge potentials and the difference between the work functions of individual semiconductors influence charge transfer [28].

To further enhance the application of Z-scheme system performance for possible industrialization, a three-component system involving an oxidation semiconductor combined with two reductive semiconductors or two oxidative semiconductors coupled with a reductive semiconductor was proposed. In 2016, Li et al reported a hydrothermal and thermo-polymerization synthesized g-C_3N_4-WO_3-Bi_2WO_6 composite for enhanced photo-electrochemical performance [52]. In their work, the conduction band electrons in WO_3 recombined with holes in g-C_3N_4 (CN) and the electrons in conduction band of CN are transferred to valence band of Bi_2WO_6. In essence, there is no major difference between either direct Z-scheme and direct dual Z-scheme or indirect Z-scheme and indirect dual Z-scheme except the increase in number of either oxidative or reductive semiconductors in dual Z-scheme composites [53,54]. According to their band alignments, three different classifications have been proposed and reportedly named as Arrow-down (Fig. 1e), Arrow-up (Fig. 1f), and Cascade (Fig. 1g) dual Z-scheme heterostructures based on their pattern shapes. The cascade pattern is described as possessing a sacrificial semiconductor that after photo-excitation all its electrons and holes are used to recombine with the useless electrons and holes in the oxidative and reductive semiconductors, respectively. Arrow-up possess two oxidative semiconductors and one reductive semiconductor increasing its oxidation ability, and arrow down has two reductive semiconductors and one oxidative semiconductor such that it has strong reductive capability.

The direct dual Z-scheme or ternary Z-scheme systems promises to be a good alternative for possible scrutiny towards industrialization. Importantly, some semiconductors may not be used to fabricate Z-scheme photocatalytic systems due to incorrect band positions of the photocatalysts for proposed use, inadequate competence for particular application, and discordant redox shuttle. The fabrication of Z-scheme photocatalytic systems should be appropriately tailored with exploration of appropriate band alignment for intended application. For example, a reduction photocatalyst should be selected such that its conduction band is more negative than $O_2/^{\bullet}O_2^-$ (-0.33 eV vs NHE) for organic pollutant degradation while an oxidative catalyst is selected such that it has enough positive potential than $OH^-/^{\bullet}OH$ (+2.29 vs NHE) for oxidation of pollutants [55,56]. Since both oxidation and reduction occurs in separate semiconductors, a semiconductor material with excellent photo-oxidation stability is suitable for use as PS II while a semiconductor with high resistance to photo-reduction is appropriate for use as PS I.

3. Verification of Z-Scheme

It has progressively become imperative to scientifically analyse the actual charge transfer that transpires at the interface of different semiconductors due to its spontaneity which birthed different heterojunctions. Here, brief, and clear discussions of the characterisation methods employed towards elucidation of Z-scheme photocatalysis are outlined with subdivisions of theoretical and experimental validation techniques.

3.1. Theoretical proof

Theoretical investigations that have been used and accepted

scientifically to provide enough evidence are simulation techniques that predict the behavioural interaction of different elemental materials input into a software. They can be employed towards structural, electronic, and interaction predictions. The parameters are important to understand different assumptions made towards establishment of the results. Density functional theory (DFT), frontier electron density calculation (FED), etc. are some of the theoretical methods that have been used for different applications [57–59]. Just recently, these theoretical investigations were employed towards validation of charge transfer in Z-scheme heterojunctions.

The DFT calculations is the most commonly used theory for different applications with different software. The detailed inspection and comparison of software performance towards a particular application would be an interesting study to actually determine the best software package to use for determining the charge transfer at the interface of two different semiconductors. With each different software, minor and major parameters are reported as they may affect the outcome of the whole process under investigation. The parameters include the module, cut-off energy, quality of k-points, and size of vacuum layer [59–61]. After the parameters are set, the most important part is the interpretation of the DFT data obtained towards understanding the interfacial charge transfer. Density of states, bandgap and work functions together with electron depletion and accumulation, and planar averaged electron density difference $\Delta\rho(z)$ along the z direction collaboratively determine electron transfer [62]. Wang et al. constructed a novel AgI/$BiSbO_4$ Z-scheme heterojunction via a hydrothermal-precipitation method towards degradation of acid red G (ARG) and tetracycline (TC) with *in-situ* generated surface plasmon resonance (SPR) from Ag^0 during degradation [62]. They employed DFT calculations to study the interfacial charge transfer at the interface of AgI and $BiSbO_4$ (Fig. 2a-e).

From Fig. 2a and b, the density of states of $BiSbO_4$ and AgI are conveyed and bandgaps of the respective semiconductors were determined as lower than the experimental values. This result is also similar to what was found by most studies that determines both experimental and theoretical bandgaps like the work of Du and co-workers [41]. Fig. 2c and d shows that AgI semiconductor donate free electrons to $BiSbO_4$ and $BiSbO_4$ shows positive value indicating it is an electron accumulation side while the negative value exhibited by AgI edicts an electron transfer route across the heterojunction. Generally, DFT calculations successfully portrayed formation of interlayer at the interface, and that the exhibited accumulation of electrons on $BiSbO_4$ after equilibrium demonstrated charge transfer from VB of AgI to $BiSbO_4$ CB. DFT calculations offer a clear insight into interfacial charge transfer that occurs between two semiconductors which can then be employed to affirm the nature of the heterojunction. More details of validation of Z-scheme charge transfer mechanism under different applications can be found in a review by Bao and co-workers on S-scheme photocatalytic systems [7].

3.2. Experimental validations

Despite theoretical investigations towards validation of Z-scheme heterojunctions formation which is normally done with DFT calculations, numerous scientific methods are employed to validate the formation of Z-scheme charge transfer mechanism in a formed heterojunction. These methods are grouped based on their mode of operation (Fig. 2f) into (1) methods used to explore chemical state of sample (metal nanoparticle photodeposition, in situ irradiated X-ray photoelectron spectroscopy (XPS)), (2) methods reflecting band energy structure (Mott-Schottky (M−S) test, UPS), and (3) methods demonstrating redox products (reactive oxygen species (ROS) generation test, photocatalytic CO_2 reduction, ESR), and just recently microscopic time resolved imaging technique [26,39,63]. The use of a single validation method may however not be sufficient and numerous methods may be required as complementary experimental or theoretical evidence for affirmation of Z-scheme charge transfer.

In metal nanoparticle photodeposition, the principle adopted is the photodeposition of noble metal co-catalysts that are described as ($M^{z+} + ze^- \rightarrow M^0$), where M is a metal ion with charge z required for its reduction to zero valence state [63]. The photoreduction is normally done on the surface of the semiconductor with the intended metal precursor with a tendency for the photodeposition to occur where there is accumulation of electrons. Since Z-scheme mechanism has distinctive reduction and oxidation sides, photodeposition will occur on the reductive or sometimes on the oxidative semiconductor [39,64]. It is possible to predict the charge transfer mechanism under light irradiation in the presence of electron donor or acceptor sacrificial agents, based on the metal photodeposition as the photo-deposited metals can be seen under TEM and mapping will show on which semiconductor the photodeposition occurred.

XPS is used for chemical composition and surface oxidation states analysis and it has also proved to be a vital technique to study the charge transfer pathway in a heterojunction by exploring the relative shift in binding energy of individual elements in the composite [65]. When a foreign material is added to a semiconductor, the binding energy shift occurs subsequent to existence of electron transfer between them, where a positive shift in binding energy validates decrease in electron density of the element while a negative shift affirms increase in electron density. Therefore, a shift in binding energy in XPS spectra can be used to confirm electron transfer mechanism at the interface of a Z-scheme heterostructure. Jo et al. reported that the decrease in the intensity and shift to higher binding energy of elements in high XPS spectra of composites compared to pristine semiconductors confirmed Z-scheme charge transfer between g-C_3N_4/TiO_2 [66].

Mott-Scotty plots have also been implemented to understand band structure of individual composites that can then be used to predict the charge transfer dynamics in Z-scheme heterojunctions [67]. However, Mott-Schottky plots are more clearly used to further elucidate and complement the radical trapping experiments. In our previous work, we showed the use of M−S plots to portray formation of direct Z-scheme heterojunction between ceria and CN [68]. The M−S plots were used to give the band structure while the radical trapping experiments gave information on most active radicals which were used together to show existence of direct Z-scheme charge transfer between CN and ceria. Comparison of possible heterojunctions with generated radicals inevitably rules out formation of some heterojunctions and thus give insights into the charge transfer route. Also some reports exist for complementary use of M−S plots to further describe charge transfer in a Z-scheme [69]. Another common technique that is employed towards systematic analysis of charge transfer mechanism in Z-scheme is UPS spectra. In short, linear approximation of the UPS spectra gives the work function of the catalysts that can be used to determine their Fermi levels and valence and conduction bands. This can then be easily employed to determine the Z-scheme charge transfer at the interface and the details of this method is given by Aguirre et al. [70]. The surface potentials of semiconductors can be measured by spectroscopic techniques such as Kelvin probe force microscopy (KPFM), surface photovoltage spectroscopy (SPS) and transient absorption spectroscopy (TAS) to affirm Z-scheme charge transfer route [39,71–73].

In radical trapping experiment, a chemical reagent is added to quench the effect of a particular set of expected radical species through capturing it [74]. Comparisons based on the activity with and without the radical trapping chemical reagent will give insights into existence and possible magnitude of the specific radical contribution [55,75]. The understanding of the involved radicals aid towards prediction of charge transfer mechanism in a Z-scheme heterojunction [75]. Since the most common initiators of photocatalytic redox reactions stems from h^+, hydroxyl radicals and superoxide anion radicals, radical scavengers for each one of them include TEOA, EDTA and ammonium oxalate (AO) for h^+ [76,77], *tert*-butyl alcohol (TBA) and isopropanol (IPA) for OH radicals [78,79], and N_2 gas and p-benzoquinone (BQ) as superoxide anion radical quenchers [76,80]. In our previous work, we proved existence of

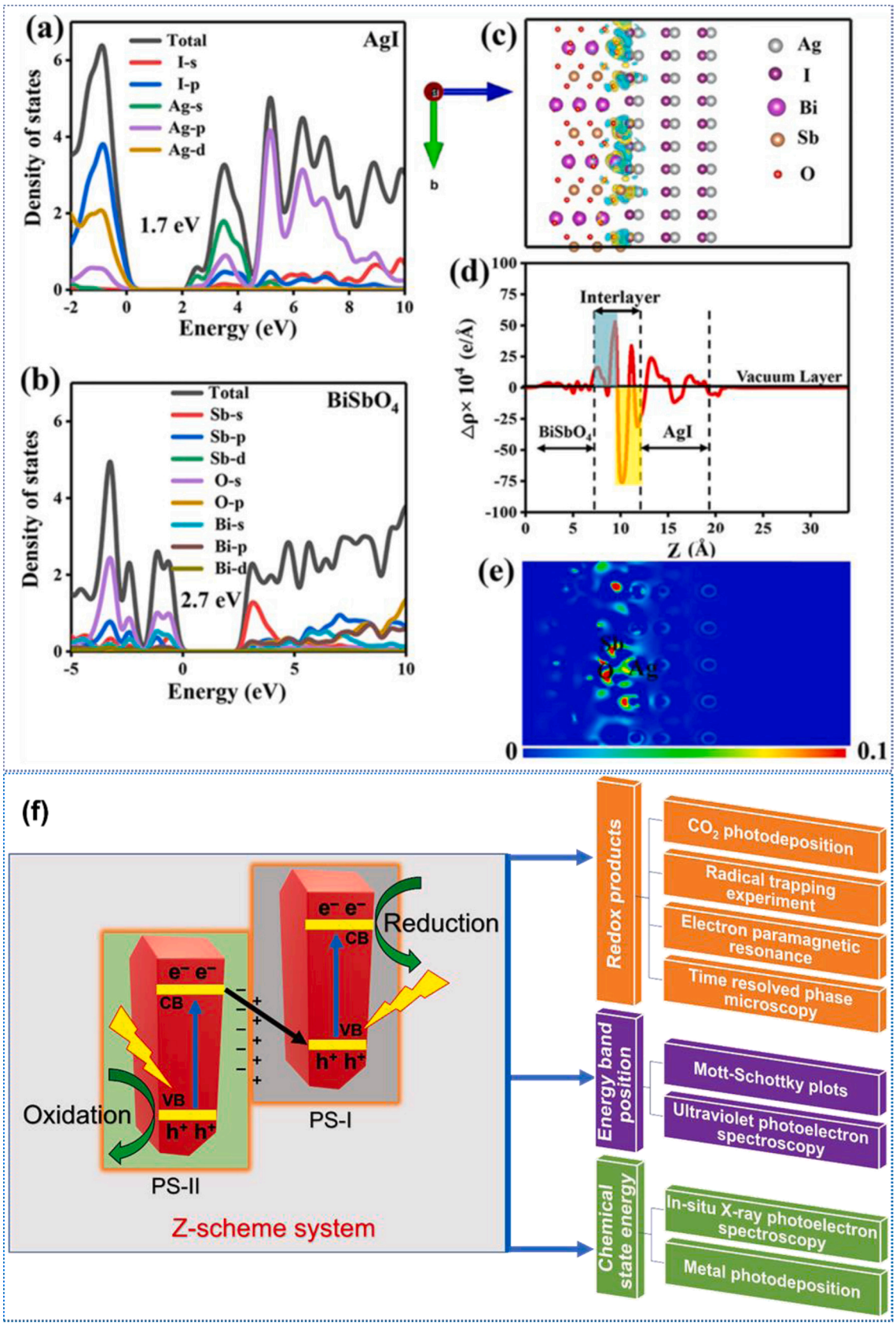

Fig. 2. TDOS and PDOS of (a) $BiSbO_4$ and (b) AgI. (c) Charge difference distribution between AgI with (0 0 2) plane and $BiSbO_4$ with (0 2 0) plane: charge accumulation is in yellow and depletion in cyan. (d) Planar averaged electron density difference Δρ (z) along the z direction of the interlayer. (e) Electronic location function (ELF) of the interlayer [62] (f) Summary of experimental validations methods of Z-scheme heterojunctions for pharmaceutical degradation and pathogens inactivation. (For interpretation of the references to colour in this figure legend, the reader is referred to the web version of this article.)

a Z-scheme charge transfer mechanism between CO_3O_4 and BiOI towards direct Z-scheme charge transfer using just radical trapping tests and some theoretical investigations that included electronic properties of the materials [74]. Similar reports exist from other groups for successful use of radical trapping experiments to confirm charge transfer pathway in Z-scheme [81].

In CO_2 photoreduction reaction, photoexcited electrons play a major role based on their conduction band edge potential energy after a heterojunction is formed. The product of a photoreduction reaction is used to predict the charge transfer mechanism when the band edge positions of the semiconductors are determined (experimentally or theoretically) such that if a traditional heterojunction is formed, the reduction in the redox capability of the semiconductor reaches a level that is undesirable for photoreduction of CO_2 to CO (-0.42 eV vs NHE), CH_3OH (-0.38 eV vs NHE) or CH_4 (eV vs NHE) [82–85]. Therefore, CO_2 photoreduction gives different products based on the reduction potential [39]. Its application towards confirmation of Z-scheme transfer mechanism is portrayed in proposed Z-scheme BiOI/g-C_3N_4 towards CO_2 photoreduction under visible light by Wang and co-workers [83]. The use of CO_2 experiment towards confirmation of Z-scheme mechanism was employed after CB and VB potentials of BiOI were 2.42 and 0.67 eV, and that of g-C_3N_4 were determined to be 2.17 and − 0.52 eV, respectively. If the photocatalytic system obeys a traditional double charge transfer mechanism, the accumulated electrons on the conduction band of BiOI would be more positive than the CO_2 reduction potentials leaving the Z-scheme as the possible charge transfer mechanism. Studies towards confirmation of Z-scheme charge transfer mechanisms are influenced by (1) the reaction products obtained and (2) the band edge potentials of the individual semiconductors.

Electronic paramagnetic resonance (EPR) is a spectroscopic technique commonly employed towards systematic investigation of charge transfer mechanism at the interface of semiconductors. Its application in the determination of Z-scheme charge transfer mechanism has largely increased over the last decade and it is based on the determination of $^{\bullet}OH$ and $^{\bullet}O_2^-$ indirectly through use of 5,5-dimethyl-1-pyrroline *N*-oxide (DMPO) as a trapping agent to generate EPR measurable DMPO-$^{\bullet}OH$ and DMPO-$^{\bullet}O_2^-$ signals [84,86,87]. The increase of the signals intensity with increase in radiation time signals generation of OH radicals and superoxide anion radicals. From the present generated radicals and the band alignment of the individual semiconductors, the Z-scheme mechanism can be assured. In a study by Xu et al. [88], a Z-scheme mechanism was confirmed to occur during sulfadiazine (SDZ) oxidation and Ni(II) reduction by a $Cu_2O/Bi/Bi_2MoO_6$ composite ruling out the possibility of p-n heterojunction formation due to determination of $^{\bullet}OH$ radicals signal in EPR that would not occur when holes concentrate on the VB of Cu_2O in traditional p-n heterojunction.

The ongoing attempts of studying charge transfer mechanism in Z-scheme resulted in novel methodology developments or modifications. Ebihara et al. applied pattern-illumination time-resolved phase microscopy towards in depth investigations that probe photogenerated charge carrier dynamics using a Mo-doped $BiVO_4$ and Rh- doped $SrTiO_3$ with indium tin oxide as the electron mediator [89]. They did not only manage to map reactive sites and recombination centres, but they also fruitfully observed position- and structure-dependency of photoexcited charge route. Therefore, characterization of Z-scheme photocatalytic systems promotes understanding that can be employed for optimisation of charge transfer and separation efficiency.

4. Z-Scheme photocatalysis

On pollutant degradation, general removal of all classes of organic pollutants has been inspected. However, given the current global pandemic outbreak of the Covid-19, it is of paramount importance to examine the applications of both direct and indirect Z-scheme charge transfer composites towards remediation of different classes of pharmaceuticals and pathogens in water bodies.

4.1. Pharmaceuticals degradation

Pharmaceuticals are classified as organic pollutants of concern by environmentalists while pharmaceuticals production and consumption has steadily escalated due to increased number of patients in need of medical attention due to sicknesses and symptoms concomitant with Covid-19 pandemic, and emotional traumas triggered by effects of the Covid-19 on the economy and freedom. Inevitable use of antiviral and antibiotic medications and their prescription has ensued their secretion into drinking water systems which is very precarious in different perspectives: (1) the pollutants bio-accumulate and their concentrations increase in drinking waters and can become deadly under acute or chronic exposures, (2) they can form extremely lethal metabolites when interacting with the ecosystem, (3) and they may result in another pandemic of drug resistance as elongated ingestion of pharmaceutical polluted water may lead to emergence of drug resistant strains of pathogens. Their removal from water bodies is justified with the use of advanced oxidation processes based heterojunctions, especially Z-scheme heterostructures formation, considered a go-to technique with possible sustainability and low cost when sunlight is used as activation energy source.

The applications of Z-scheme systems have increased exponentially in the past decade for pharmaceuticals pollution remediation because of their ability to reserve the strong redox capability of oxidative and reductive semiconductors, improved charge separation efficiency, and provision of distinctive redox reaction sites for high photoactivity. It has numerous fabrication strategies that have to be observed for better performance in pharmaceutical degradation. The staggered band alignment, and intimate contact or a charge transfer channel are required during construction of the Z-scheme charge transfer heterostructures [10,35,90]. The charge transfer channel in traditional Z-scheme systems entails utilization of reversible redox ion pairs in liquid phase which has not been largely applied in water treatment as some pollutants are either electron acceptors or donors that would quench the effective charge transfer mechanism in this system. All-solid-state Z-scheme heterostructures normally employ the use of solid redox mediators (SRMs) and they are employed for degradation of pharmaceuticals and pathogens inactivation. Direct Z-scheme encompass the generation of a direct contact between the semiconductors which is aided and enhanced by internal electric field (IEF), interfacial defect states, and selective facet design [35]. In essence, the optimisation of Z-scheme systems can be achieved by enhancing the charge transfer at the interface of the semiconductors. In indirect Z-scheme, the optimisation of the catalyst ratios and the amount of solid redox mediator forms an integral aspect for enhancement of charge separation efficiency which in turn boosts the photocatalytic performance [91]. Except the universal optimisation conditions (catalyst amount, reactor design, amount and pH of pollutant, photons flux, etc.), direct Z-scheme heterostructures performance is boosted immensely through an intimate hetero-interface contact with low charge resistance that is established through Coulomb electrostatic interaction, van der Waals (vdW) forces, hydrogen bonding, and chemical bonding [91]. Coulomb electrostatic interaction are physical mechanisms induced by negative and positive charged particles electrostatic adsorption, hydrogen bonding results in low resistance interfaces induced by hydrogen bonds, and van der Waals (vdW) forces emerge from strong interaction and distinctively formed face-to-face contact of 2D layers which facilitate interfacial charge transportation with low charge resistance heterointerfaces [92,93]. This ensures the popularity of direct and indirect Z-scheme systems towards pharmaceuticals degradation and pathogens destruction from water with comparative data of conditions and efficiency summarised by Table 1. Dual-Z-scheme heterostructures promises to be very effective compared to single direct or indirect Z-scheme heterojunctions due to (1) the increase in the redox capability of the system by increasing either its oxidation power or reduction power, and (2) the systematic growth of catalytic reaction centres which upturns degradation performance

Table 1
Different Z-scheme photocatalytic systems for remediation of pollutants and bacterial inactivation under different conditions.

Composites	Synthesis method	Charge transfer Mechanism	Conditions (source of light, efficiency, type of pollutant, irradiation time)	Refs
AgI/Ag/Bi_3TaO_7	Ultrasonic assisted precipitation-photoreduction	Indirect	−300 W xenon lamp (UV filter); 98.37 %; sulfamethoxazole; 12 min −85 %; oxcarbazepine; 60 min	[29]
g-C_3N_4/ $Bi_4Ti_3O_{12}$/ $Bi_4O_5I_2$	Hydrothermal	Dual indirect	500 W Xe lamp (240 mW cm^{-2}, λ > 420 nm); 87.1 %; ofloxacin; 90 min	[94]
AgBr/$LaNiO_3$/g-C_3N_4	Ultrasound-assisted hydrothermal	Hybrid direct and indirect	500 W xenon lamp (λ > 420 nm); 92 %; norfloxacin; 2 h	[95]
$LaNiO_3$/g-C_3N_4	Facile heat treatment	Direct	visible light (λ > 420 nm);- 96 %; tetracycline; 300 min	[96]
MOFs-derived Black Phosphorus QDs/ Cu_2O/*N*-doped hollow porous carbon	Ultrasonication-assisted solvothermal	Indirect	a 300 W Xenon lamp (λ > 420 nm) 99.99999 %; Methicillin-resistant Staphylococcus aureus; 30 min	[97]
Ag/g-C_3N_4/Bi_3TaO_7	In-situ growth method	Indirect	300 W xenon lamp; 98 %; sulfamethoxazole; 25 min	[56]
Bi_2S_3/$BiVO_4$/$MgIn_2S_4$	hydrothermal method using an electrostatic self-assembly	Direct dual	300 W xenon lamp (λ > 400 nm); 99 %; carbamazepine; 20 min	[90]
N,S-CQDs/Bi_2MoO_6@TiO_2	Hydrothermal	Indirect	visible light (λ > 400 nm, 273.1 mW/cm^2); 85.8 %; ciprofloxacin; 240 min NIR light (λ > 700 nm, 109.6 mW/cm^2); 85.8 %; 44.6 %; ciprofloxacin; 240 min visible light (λ > 400 nm, 273.1 mW/cm^2); from 7.56-log to 1-log cfu/mL; B. subtilis and E. coli; 1.5 h	[98]
Bi_2MoO_6/ Bi_2WO_6\ AgI\Ag	Isoelectric point and continuous ion layer adsorption	Dual direct	300 W Xenon lamp; 94.85 %; malachite green; 180 min	[99]
α-Fe_2O_3/g-C_3N_4	controlled crosslinking and hydrolysis	Direct	300 W Xenon lamp (λ > 420 nm); 67 %; tetracycline, 2 h	[100]
Nitrogen-doped carbon dot (NCD) Bi_2MoO_6/g-C_3N_4	Hydrothermal	Indirect	8 × 8 W visible lamps; (λ = 380–580 nm); 99 %; ciprofloxacin; 30 min	[101]
Co_3O_4/$CuBi_2O_4$/$SmVO_4$	Ultrasonication	Dual direct	300 W Xe lamp with AM1.5G filter (λ = 350–1100 nm); 76.1 % ± 3.81; carbamazepine; 300 min	[102]
AgI/$Zn_3V_2O_8$	Hydrothermal	Direct	Sunlight/permonosulfate (PMS); 93 %, 90.1 %, and 89.4 % for tetracycline, oxytetracycline, and doxycycline; 20 min	[50]
Ag_3PO_4/Bi_2S_3/Bi_2O_3	Hydrothermal and Solvothermal	Dual direct	300 W Xenon lamp (λ > 420 nm, 100mWcm^{-2}); 98.06 % and 90.26 %; sulfamethazine and cloxacillin; 90 min	[103]
$ZnIn_2S_4$/MoO_3	Impregnation	Direct	visible light (λ ≥ 420 nm); 87 %; paracetamol; 100 min	[104]
g-C_3N_4/m-Bi_2O_4	Hydrothermal	Direct	Xenon lamp (300 W, λ less than 400 nm); 100 %; Escherichia coli (E.coli K-12); 1.5 h	[105]
O-g-C_3N_4/HTCC (hydrothermal carbonation carbon)	facile low-temperature solvothermal-hydrothermal	Direct	7 W-white light emitting diode (LED) lamp (40 mW/cm^2, λ > 400 nm); 100 %, human adenovirus type 2 (HAdV-2); 120 min	[106]
g-C_3N_4/WO_3/AgI	Electrostatic self-assembly plus selective deposition	Dual direct	300 W Xenon lamp; 95.2 %; nitenpyram, 5 min	[53]

despite tumbling the potential upscaling of the system due to cumulative cost. In this section, the degradation of pharmaceuticals with Z-scheme heterojunctions with exhaustive analysis focused on antibiotics and non-steroidal anti-inflammatory drugs (NSAIDs) is explored.

Except the formed heterojunction in the composite that is used for pharmaceutical degradation, important factors during the process needs to be taken into consideration and optimised as they can negatively affect the efficiency of the process. These factors can be grouped into (1) conditions of the photocatalytic reaction reactor and (2) properties of the materials. The degradation of pharmaceuticals requires the reactor volume to be appropriate for the intended application and since one of the most important requirements is adequate interaction of pollutant and catalyst, stirring is important to enhance the adsorption of the pollutant on the catalyst surface [107]. Adsorption should be allowed to occur for a certain period of time until it reaches equilibrium. Moreover, the source of the reactor light is an important aspect as UV and visible light is required to initiate electrons and holes pairs formation in the Z-scheme heterojunction for generation of radicals that pioneer photocatalytic reactions [90,107]. The proximity and energy of the light source determines photons flux and energy absorption by the catalyst. The source of light to be employed is determined by the optical properties of the individual or composite semiconductors as UV or visible light active semiconductors require UV or visible light sources, respectively. The semiconductor and the pollutant should possess different charges (positive and negative) to allow Coulomb force induced attraction for enhanced pollutant adsorption on catalyst. The pharmaceutical pollutant charges in water solutions are normally determined by their PKa which in influenced by solution pH and is negative or neutral in pH values higher and lower than the PKa value, respectively [106]. Moreover, the solution volume and concentration ratio to catalyst concentration should be optimised while other factors such as temperature and pH of solution, and the composition of the pollutant solution are of paramount importance. The presence of cations and anions may compete for adsorption sites with positive or negatively charged pharmaceutical pollutants and retard degradation efficiency. The presence of certain anions may also retard photocatalytic degradation efficiency by scavenging the robust hydroxyl radicals to form other radicals that are less reactive such as OH radicals quenching with chlorine containing anions [101].

4.1.1. Antibiotics

Generally, antibiotics are classified as persistent organic pollutants, they are non-biodegradable and can persist in the environment causing harmful effects to human health. In recent studies on photocatalysis, emerging pollutants such as pharmaceuticals are being used as model water pollutants with some reviews focusing on the degradation of these materials using specific semiconductors such as Bi_2WO_6 based photocatalysts grouping the antibiotic pharmaceuticals into three different classes of sulfonamide antibiotics, tetracycline antibiotics [108] and fluoroquinolones antibiotics [109] which is adopted in this review for systematic and in depth analysis of Z-scheme heterojunctions towards degradation of antibiotics. These antibiotics are widely employed for deterrence and cures of photogenic diseases that have immensely escalated during Covid-19 pandemic ensuing their predominant determinations in water bodies.

Fluoroquinolones (FQ) antibiotics are subclass of quinolones and

they have characteristic fluorine atom in the central ring system. Fluoroquinolones are widely used against a range of bacterial infections such as typhoid fever, and sexually transmitted diseases. The examples of detected fluoroquinolones in water systems that have been studied for possible degradation with Z-scheme heterojunctions include norfloxacin, levofloxacin, ciprofloxacin, and ofloxacin. Ofloxacin is a widespread FQ antibiotic used for the treatment of skin, urinary and respiratory infections, gonorrhoea, pneumonia, and bronchitis. Kumar et al. degraded ofloxacin under visible light irradiation with dual Z-scheme g-C_3N_4/$Bi_4Ti_3O_{12}$/$Bi_4O_5I_2$ heterojunction which possessed I_3^-/I^- and Bi^{3+}/Bi^{5+} and redox mediators synthesised through the hydrothermal route [94]. M−S plots were used to determine the conduction band positions of the semiconductors towards proposal of charge transfer mechanism at their interfaces, and to show that all the semiconductors were *n*-type semiconductors as their slopes on the M−S plot is positive (Fig. 3a). The photocatalytic experiments were conducted in a gas circulation and pumping system connected Pyrex reactor with autosampler. Anaerobic conditions were induced through pumping dissolved oxygen with vacuum before the experiment began. A 500 W Xe lamp (240 $mWcm^{-2}$) with 420 nm cut-off filter irradiated a 100 ml solution of 10 mg L^{-1} with 45 mg of photocatalyst during degradation process. 87.1 % ofloxacin (OFL) removal efficiency was obtained in 80 min which was indexed to electron separation and formation of Z-scheme mechanism as shown by EIS Nyquist plots (Fig. 3b), transient photo-current response (Fig. 3c), and photoluminescence spectra (Fig. 3d). The degradation pathway of OFL was proposed to result in CO_2, H_2O, and NH_3 upon complete mineralization. M−S plots, ESR, and radical scavenging experiments were used to confirm the formation of Z-

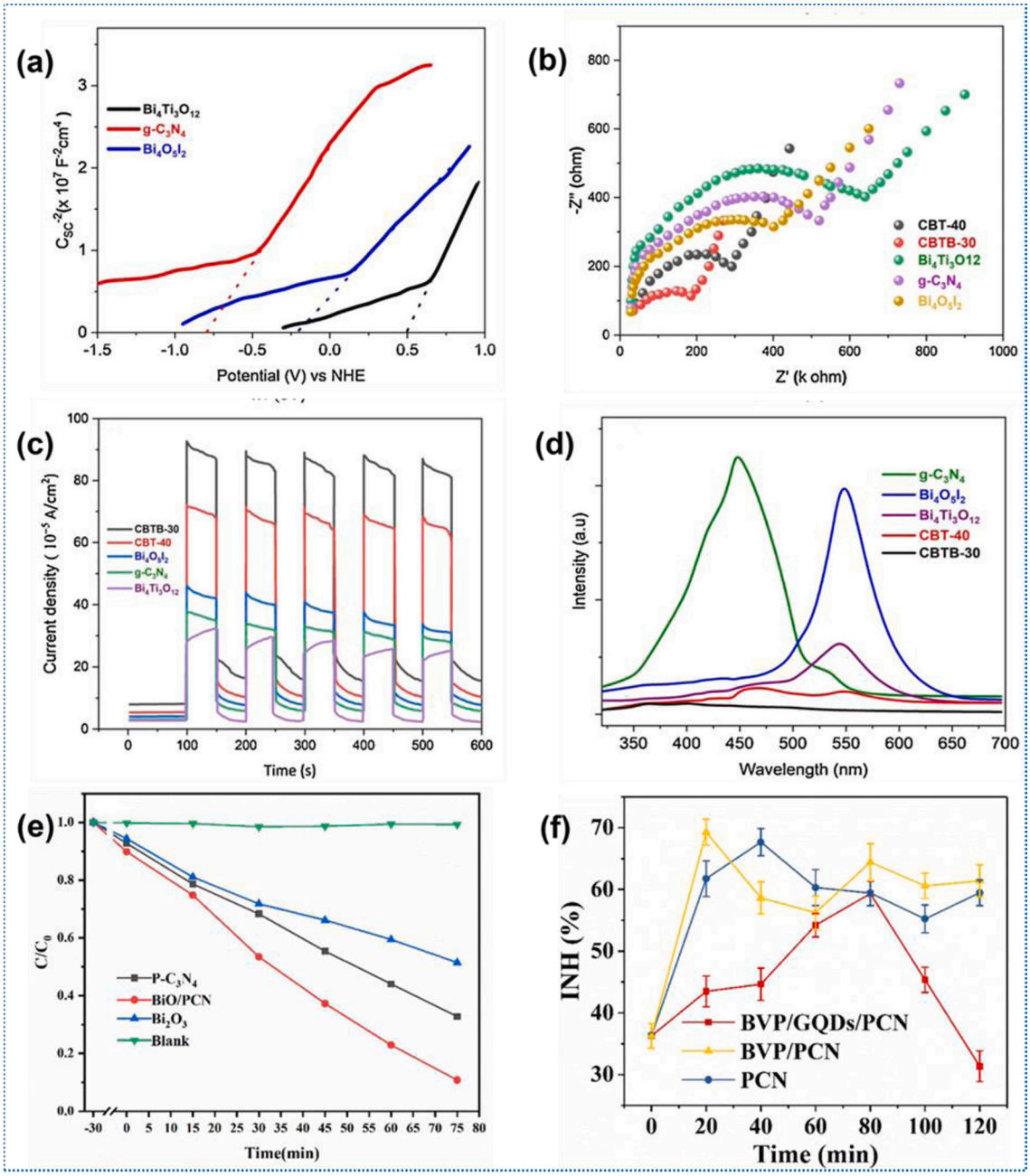

Fig. 3. (a) Mott-Schottky plots, (b) EIS Nyquist plots, (c) transient photo-current response, (d) photoluminescence spectra of synthesised dual Z-scheme g-C_3N_4/$Bi_4Ti_3O_{12}$/$Bi_4O_5I_2$ heterojunction [94], (e) levofloxacin degradation rate of the synthesised S-scheme heterojunction Bi_2O_3/P-C_3N_4 photocatalyst [110], and (f) the luminescence inhibition (INH) of the bioluminescence of V. fischeri at different reaction time [111].

scheme mechanism in this work with numerous effects of different parameters explored on the degradation of OFL. The ESR was used to affirm the formed ROSs in this photocatalytic system by identifying the changes during DMPO trapped •OH and $\bullet O_2^-$ compared in the presence and absence of light irradiation under optimum conditions in 10 min. In the dark, no signals were observed while the signals of characteristic 1:2:2:1 quadruple for •OH surpassed that of DMPO-$\bullet O_2^-$ after light irradiation suggesting that •OH are major influencing radicals for photodegradation of OFL. Additionally, radical trapping experiments further affirmed the major involvement of OH radicals. Under aerobic conditions, dissolved oxygen reacts with photogenerated electrons forming $^{\bullet}O_2^-$ with the rate determining step assigned as the electron transfer to O_2.

The degradation of other fluoroquinolones has been reported in literature recently. An efficiency of 89.2 % during levofloxacin degradation was achieved in 75 min under simulated solar radiation on Bi_2O_3/P-C_3N_4 direct Z-scheme nanocomposite (Fig. 3e) with improved hydrophilicity and BET surface area [110]. Density functional theory, (DFT), ESR, and radical trapping experiments were used collaboratively to affirm the charge transfer mechanism at the interface of the semiconductors to be Z-scheme. A DFT analysis was performed to determine the work functions of the semiconductors with that of Bi_2O_3 higher than that of P-C_3N_4 while band bending occurred downwards and upwards (due to electrons loss in P-C_3N_4). The synergy between energy band bending and in-built electric field generate a pathway for rapid recombination of electrons from Bi_2O_3 and holes from P-C_3N_4 for efficient charge separation and maintenance of strong redox capability of the direct Z-scheme system. Z-scheme degradation of levofloxacin has also been reported with an efficiency of 90.8 % in 70 min of irradiation on Sm_6WO_{12}/g-C_3N_4 nanocomposite through $^{\bullet}O_2^-$ and •OH as the main ROSs [112]. Moreover, ciprofloxacin degradation was accomplished with an indirect Z-scheme Bi_2MoO_6/g-C_3N_4 with nitrogen doped carbon dots as the electron mediator [101]. The Z-scheme mechanism was proved with ESR and radical trapping experiments while the effect of solution pH, initial concentration of CIP, catalyst dosage, and inorganic anions and organic matters were studied. The pH 8 of the solution, 1 mgL^{-1} initial solution concentration, and 1.0 gL^{-1} of catalyst dosage gave the highest photocatalyst performance. Similarly, to dissolution of organic constituents, inorganic anions broadly exist in water and were reported to inhibit degradation performance of the catalyst, and the main given reason was completion of active sites and also scavenging of radicals by anions where new radicals with less oxidising power can be formed Eq. (1)-(4).

$$NO_3^- + \cdot OH \rightarrow \cdot NO_2^- + 1/2O_2 + OH^- \quad (1)$$

$$HCO_3^- + \cdot OH \rightarrow \cdot CO_3^- + H_2O \quad (2)$$

$$Cl^- + \cdot OH \rightarrow \cdot ClOH^- + H_2O \quad (3)$$

$$H_2PO_4^- + \cdot OH \rightarrow \cdot HPO_4^- + H_2O \quad (4)$$

The degradation of norfloxacin was also examined with direct dual [32] and indirect Z-scheme mechanisms [111] with $BiFeO_3$/$CuBi_2O_4$/$BaTiO_3$ and phosphate-doped BiVO4/graphene quantum dots/P-doped g-C_3N_4 (BVP/GQDs/PCN) under visible light irradiation with efficiencies of 93.2 % and 86.3 % within 60 and 120 min, respectively. Evidently, the degradation time incurred during photodegradation of this class of antibiotics reach a maximum of 2 h towards high mineralization efficiencies that are enticing for industrial applications of Z-scheme heterojunctions towards large-scale applications of antibiotics degradation in water. The incomplete degradation was studied with bioluminescence inhibition assay and portrayed that highly toxic intermediates were formed (Fig. 3f) during the use of the Z-scheme heterojunction.

Tetracycline antibiotics are cheap and widely used antibiotic pharmaceutical agents which is not surprising that they are widely studied for their photocatalytic degradation in environmental waters including with Z-scheme photocatalysts [48]. The Mott–Schottky (M−S) plot was employed for examination of band structure towards confirmation of Z-scheme heterostructure in conjunction with radical trapping experiments for both BiOCl and Bi_2O_3 samples also providing information on whether the semiconductors are p-type or *n*-type [113]. The positive slopes indicated that the semiconductors are *n*-type and it was further employed to determine band edge positions of the semiconductors to compare with radical experiments to substantiate the interfacial charge transfer to follow indirect Z-scheme with Bi as the electron mediator between BiOCl and Bi_2O_3. There are numerous photodegradation experiments that have been conducted with different photocatalytic Z-scheme heterojunctions towards degradation of single [10,107,114] and multiple [115] tetracycline antibiotics in water. Dual direct Z-scheme MoS_2/g-C_3N_4/$Bi_{24}O_{31}Cl_{10}$ ternary heterojunction was evaluated towards degradation of TC with 97.5 % degradation efficiency in 50 min of visible-light irradiation by Kang and co-workers [86]. PL spectra, time-resolved PL spectra, photocurrent response and EIS spectra (Fig. 4a-d) synchronously proved the charge separation in the composite compared to pristine semiconductors with reduced PL intensity, increase in average lifetime of photogenerated charges, highest photocurrent intensity, and small charge transfer resistivity, respectively. EPR and radical quenching experiments confirmed the formation of Z-scheme charge transfer mechanism. The EPR signal of DMPO-$^{\bullet}O_2^-$ was observed after 5 min of irradiation time while the DMPO-•OH signals were observed after 10 min signalling that the $^{\bullet}O_2^-$ radicals are the main reactive species in TC degradation.

Sulfonamide antibiotics are characterized by the presence of amide of sulfonic acid and they are normally employed as antibacterial, anticonvulsant, anti-inflammatory, and diuretic humans or livestock drugs. Their determinations in water matrix are gaining momentum yearly due to their demand and their detections in the environment are increasing due to their resistance to biodegradation and their bio-accumulative nature imperilling aqualife, human health, and the ecosystem. Z-scheme AgI/$Bi_4V_2O_{11}$ heterojunction was synthesized by Wen and co-workers towards visible light degradation of sulfamethazine (SMZ) with an efficiency of 91.47 % in 60 min of irradiation [18]. SMZ degradation in presence of Cl^-, SO_4^{2-}, NO_3^-, and HCO_3^- portrayed inhibitory effect on the efficiency of SMZ degradation from 93.17 % to 80.44 % and 54.22 % during 60 min in the presence of Cl^- and HCO_3^-, respectively (Fig. 4e). The minor efficiency decrease in the presence of chloride ions could be mainly due to competition of active sites between chloride ions and pollutant on the surface of the catalyst while HCO_3^- works as a scavenger to trap and convert active ROSs into less oxidative or reductive radicals lowering the overall efficiency of the system.

The systematic study of the re-used products showed that the crystal structure and the elemental composition of the composites did not change as analyzed by XPS (Fig. 4f) with further analysis of the Ag^+ peak showing that no Ag^0 was formed. Similar degradation of SMZ together with cloxacillin (CLX) were performed with dual direct double Z-scheme Ag_3PO_4/Bi_2S_3/Bi_2O_3 under visible light radiation with 98.06 % and 90.26 % efficiency in 90 min, respectively [103].

Xu et al fabricated a direct Z-scheme 0D/1D AgI/MoO_3 photocatalyst towards visible light driven degradation of sulfamethoxazole (SMX) with 97.6 % efficiency in 20 min [30]. ESR generated DMPO-$^{\bullet}O_2^-$ and DMPO-•OH, and radical trapping experiments confirmed the formation of direct Z-scheme heterostructure which achieved mineralization of SMX as proved by 3D excitation-emission matrix (EEM) spectra and HPLC-MS spectra. From the EEM spectra (Fig. 5a-d) as irradiation progressed, the peak intensity began to fade away to signal successful degradation of SMX until the weakest intensity at 20 min showing almost complete degradation of SMX in agreement with 97.6 % calculated efficiency with the optimum composite.

A dual direct Z-scheme Ag_2S/Bi_2S_3/g-C_3N_4 heterojunction was investigated for visible light and solar light irradiation of SMX with degradation efficiency of 97.4 % in 90 min initiated by hydroxyl and

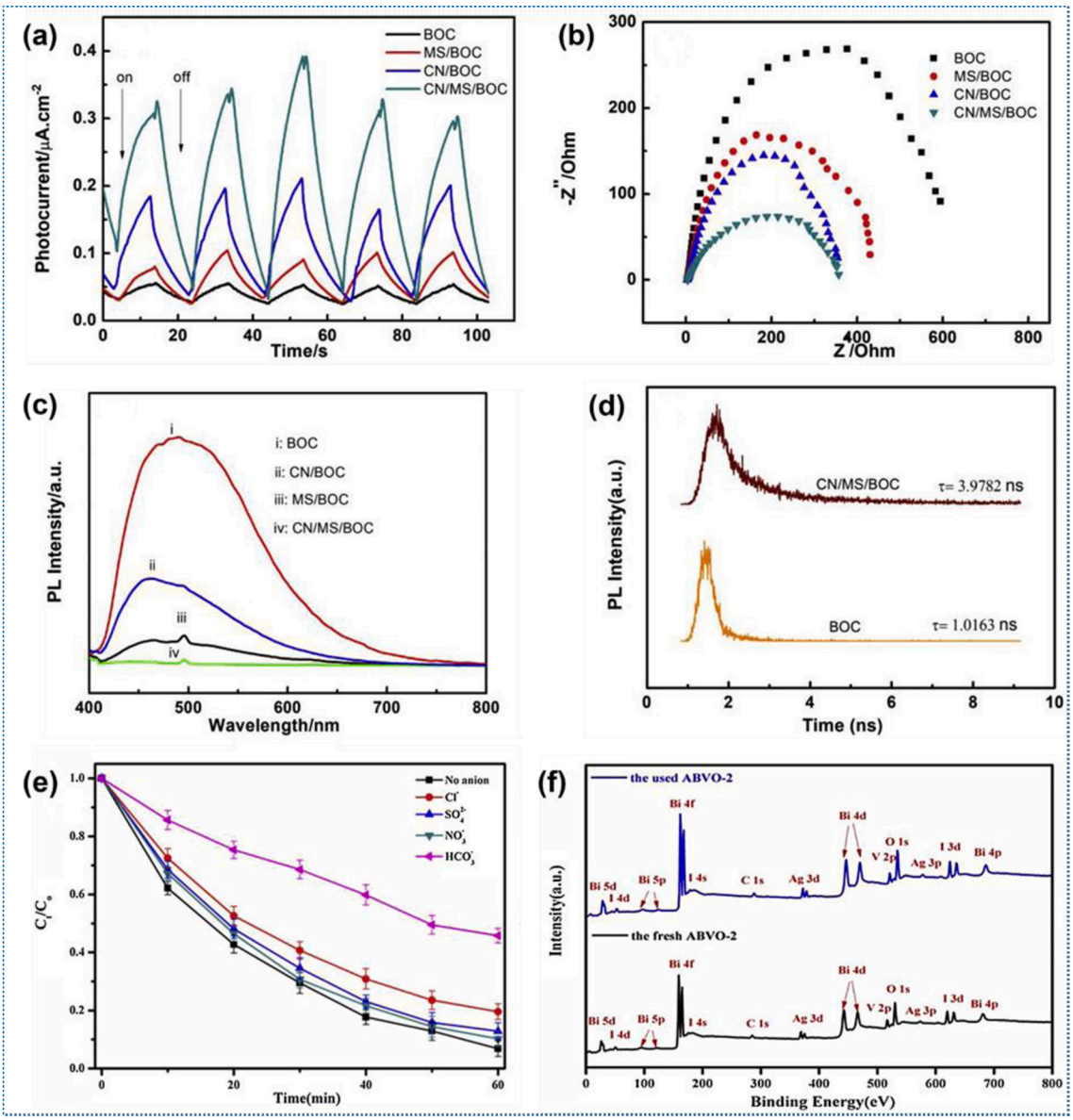

Fig. 4. (a) Photocurrent response, (b) EIS spectra, (c) photoluminescence spectra excited at 360 nm and (d) time-resolved PL spectra of dual Z-scheme MoS_2/g-C_3N_4/$Bi_{24}O_{31}Cl_{10}$ ternary heterojunction photocatalysts [86], (e) Effect of different inorganic anions on SMZ degradation by direct Z-Scheme AgI/$Bi_4V_2O_{11}$ photocatalyst ([anions concentration] = 10 mM; [Catalyst dosage] = 0.1 g/L; [SMZ] = 10 mg/L); and (f) Comparison of the survey XPS spectra of the used and fresh catalyst after 60 min of visible light degradation [116].

superoxide anion radicals with in-situ generation of Ag as electron shuttle as proved by XPS [117]. The degradation pathway was investigated with LC–MS analysis after 30 min and 90 min of SMX degradation with the optimum performing catalyst under visible light showing all the intermediates that were used to predict the degradation reaction pathway. No aliphatic compounds were detected and the TOC results proved high mineralisation efficiency of 67.4 % and 85.1 % at 30 °C under solar and visible light irradiation after 120 min.

Other classes of pharmaceuticals have also been investigated for removal from water environment with Z-scheme heterojunctions. Carbamazepine is one of the pharmaceutical and personal care products (PPCPs) that is classified as an anticonvulsants/antiepileptics [118] capable of causing detrimental effects to human health and the environment despite some of its important medicinal uses in treating trigeminal neuralgia, epilepsy or other diseases [119]. In our group, we constructed a dual Z-scheme Co_3O_4/$CuBi_2O_4$/$SmVO_4$ photocatalyst towards visible light driven degradation of carbamazepine (CBZ) with attained efficiency of 76.1 % within 300 min of irradiation [102]. The bandgap energies attained from UV–vis and the CB edge potentials estimated by XPS were used to draw up the energy diagram with band positions for the involved semiconductors. The radical scavenging tests affirmed involvement of holes, $^{\bullet}O_2^-$, and $^{\bullet}OH$ towards degradation of CMZ which was then used to show that in a traditional type II interfacial charge transfer, it would be impossible to form all the ROSs leaving only the probable mechanism as the dual Z-scheme. The changes in binding energies of the system was also observed when comparing high-resolution XPS spectra of pristine semiconductors to that of the composite which depicted electron acceptor and donor semiconductors from decrease and increase in binding energy, respectively. The change in chemical environment is the phenomena behind this and the direction of electron transfer was obtained after observed increase and decrease in the binding energy of elements.

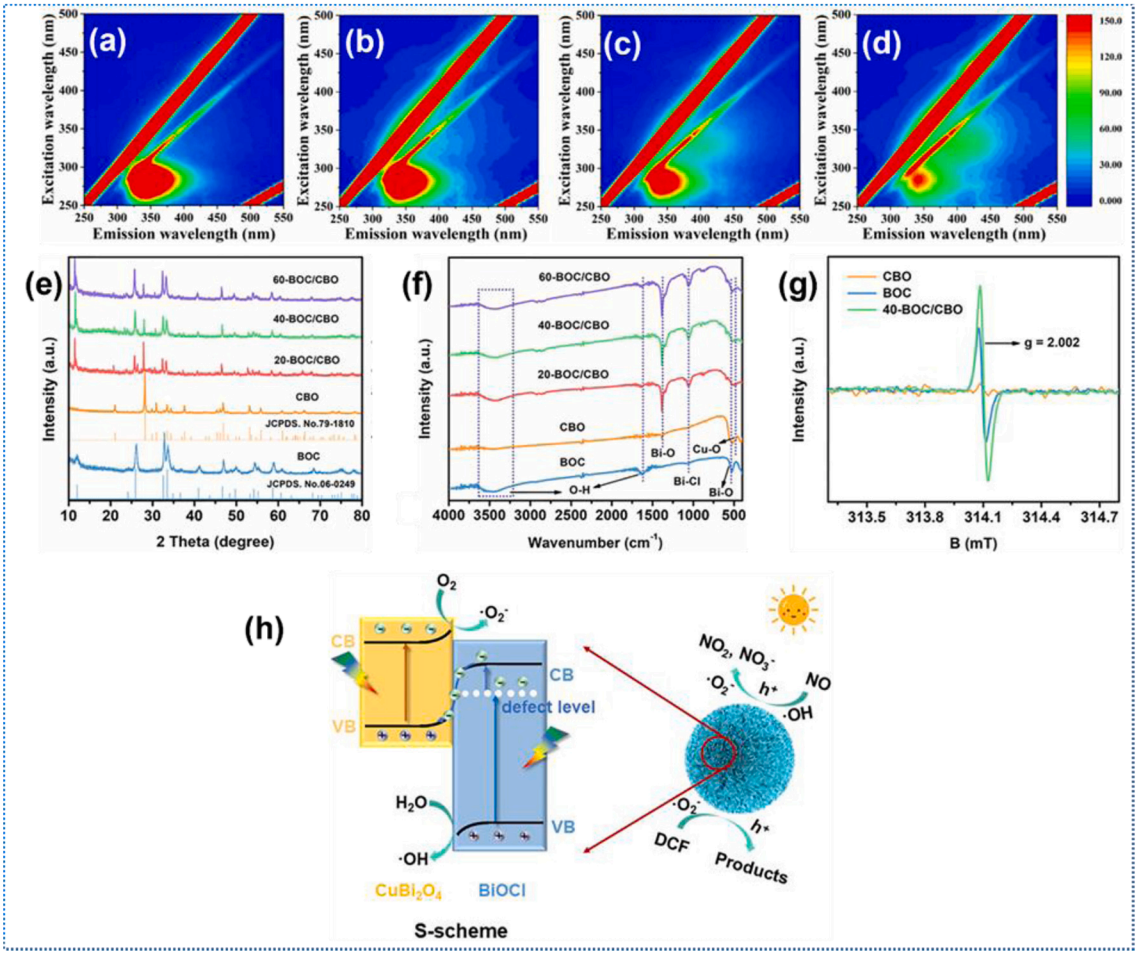

Fig. 5. the 3D EEM spectra of the SMX solution in AgI/MoO_3 visible system: (a) 0 min, (b) 5 min, (c) 15 min, (d) 20 min [30], (e) XRD patterns and (f) FT-IR spectra of as-synthesized samples (g) ESR spectra of composites, and (h) schematic illustration of a possible charge transfer mechanism for BiOCl/$CuBi_2O_4$ S-scheme heterojunction [123].

4.1.2. Nsaids

The most common non-steroidal anti-inflammatory drugs found in water media are ibuprofen (IBU) and diclofenac (DFC) with expected escalated uses due to their low cost and high functionality towards treatment of health-related issues. DFC is a NSAID engaged for inflammation treatment and most frequently administered for pain relief in humans and animals with expected usage escalations in the course of the Covid-19 pandemic [120,121]. IBU is a non-steroidal anti-inflammatory drug (NSAID), entrusted with pain and fever relief, arthritis, and to treat inflammation of minor injuries since its first introduction in 1969, being recently selected as the safest NSAID by spontaneous consumption which has surpassed 200 tons per year [122].

The existence and detections of both DFC and IBU in drinking water systems has influenced their removal from water bodies to provide clean and safe drinking water to humans. Wu et al. constructed a BiOCl/$CuBi_2O_4$ S-scheme heterojunction for visible light driven removal of diclofenac through the solvothermal method with 90 % efficiency in 60 min [123]. XRD results (Fig. 5e) and FTIR spectra (Fig. 5f) confirmed the formation of BiOCl/$CuBi_2O_4$ composites with strong interfacial contact that was proved by decrease in peak intensity of tetragonal $CuBi_2O_4$ and increase in peak intensity of tetragonal BiOCl in XRD spectra. Electron spin resonance (ESR) spectroscopy was used to investigate the formation of oxygen vacancies in the samples and the results confirmed formation of oxygen vacancies in BiOCl and BiOCl/$CuBi_2O_4$ with the intensity higher (meaning high concentration of oxygen vacancies) in the composite than pristine BiOCl (Fig. 5g). Defect-assisted charge transfer mechanism was envisaged to enhance charge transfer efficiency at the interface of the formed S-scheme heterostructure. Similarly, ESR was employed to further determine the charge transfer mechanism at the interface of the semiconductors heterostructure in combination with photoluminescence (PL), electrochemical impedance spectroscopy (EIS), radical scavenger tests, transient photocurrent response, and time-resolved fluorescence (TRPL) measurements. From the affirmed S-scheme heterojunction in this study (Fig. 5h), no distinctive difference exists with other direct Z-scheme reported mechanisms.

Ibuprofen degradation with direct Z-scheme Co_3O_4/BiOI was performed by our group together with a mixture of trimethoprim under visible light with efficiency of 97.02 % in 100 min while the degradation of only IBU was achieved in 60 min with 99.98 % efficiency. Self-assembled Co_3O_4 spherical rings were engulfed by flower like BiOI towards strong interaction and efficient separation of charge carriers studied with PL analysis [74]. Another direct Z-scheme photocatalyst was inspected for IBU degradation using Bi_5O_7I-MoO_3 photocatalyst with 89.2 % degradation efficiency in 120 min under visible light irradiation [124]. Analysis of different water matrixes incurred low reductions in photocatalytic activity of the Z-scheme composites showing that the formed Z-scheme heterojunction activity is suppressed by complex compositional contents of the real wastewater samples under investigation. However, the catalyst was still stable to some extend with stability tests confirming that it can be reused five times with less than 5 % decrease in efficiency. Some traces of adsorbed IBU after

degradation and some reduction and shifting of IR peaks and XRD peaks confirmed that adsorbed pollutant was present on the catalyst surface after degradation, proving that the catalyst can be inactivated after prolonged usage.

Wei et al. designed dual direct Z-scheme α-$SnWO_4$/UiO-66(NH_2)/g-C_3N_4 with visible light induced photodegradation of IBU attaining 95.5 % degradation efficiency within 2 h [125]. The W, O and Sn binding energies shifted to higher values in α-$SnWO_4$/UiO-66(NH_2)/g-C_3N_4 compared with $SnWO_4$ (α-SW), suggesting a strong interaction that proved the formation of a heterojunction. The kind of formed heterojunction was determined first by calculation of the bandgaps of the materials using UV–vis data and the results were 2.62, 2.51, and 1.78 eV for CN, UiO-66(NH_2) and α-SW, respectively. This showed that all the individual semiconductors absorb light in the visible range of the solar spectrum. Then M−S plots were used to respectively classify CN, UiO-66 (NH_2), and α-SW as p-, p-, and *n*-type semiconductors due to negative and positive slopes, the values of which were used to determine the flat band (E_{FB}) potentials in consideration with the Nernst's equation ($E_{NHE} = E_{Ag/AgCl} + 0.21$). The values of −0.91 and −0.5 eV (vs NHE) were calculated as conduction bands for CN and UiO-66(NH_2) while the α-SW valence band was + 2.66 eV (vs NHE). The relationship of ($E_{VB} = E_{CB} + E_g$) was employed to determine the corresponding valence and conduction band edge potentials. Similar steps have been followed with other Z-scheme semiconductors to calculate respective band edge positions experimentally using M−S plots [126]. Moreover, scavenger tests were conducted with BQ, IPA and OA for $^{\bullet}O_2^-$, $^{\bullet}OH$ and h^+, respectively to confirm generation of $^{\bullet}O_2^-$ and $^{\bullet}OH$ ROSs in the heterostructure and their involvement thereof in the photodegradation of IBU. ESR results also corroborated the radical scavenger experiments signalling that no radicals formed in the dark while peak intensities of $^{\bullet}O_2^-$ and $^{\bullet}OH$ radicals increased proportionally to increase in irradiation time inducing the proposed dual Z-scheme mechanism. Both the inorganic CN and UiO-66(NH_2) semiconductors acted as reduction semiconductors while the inorganic α-SW acted as an oxidative semiconductor ensuring provision of distinctive reaction sites for reduction and oxidation reactions respectively. Despite the increased charge transfer and separation enhancement, the redox ability of the heterojunction was higher than it would be if the traditional p-*n*-p heterojunction formed between the composites. The electrons would all accumulate on the conduction band of α-SW (+0.88 eV) while the holes would accumulate on the valence band of CN (+1.71 eV). Evidently, if this was to happen, the formation of the detected ROSs in this wok would not be possible due to inappropriate energies of electrons and holes towards respective formation of $^{\bullet}O_2^-$ and $^{\bullet}OH$. It can be inferred that based on numerous discussions in this review, Z-scheme catalyst are promising heterostructures towards general photocatalytic applications in respect to quantum efficiency, charge separation efficiency, and photoactivity.

4.2. Activation of persulfate

Application of sulfate radical ($SO_4^{\bullet-}$, E = 2.5–3.1 eV, half-life: 30–40 μs) based advanced oxidation processes (SR-AOPs) has been regarded as a hotspot of innovative research towards environmental pollution remediation [127]. The production of sulfate radicals is achieved through activation of peroxymonosulfate (HSO_5^-, PMS) or peroxydisulfate (PDS, $S_2O_8^{2-}$) by either homogeneous or heterogeneous photocatalysts [128,129]. Most recently, Z-scheme photocatalysts are used for heterogeneous activation of persulfate in photocatalytic removal of various water pollutants [127,130,131]. In heterogeneous activation of PMS/PDS, the other component if not both should be a metal or metals (Co, Mn, Fe, Cu, etc.) that can effectively break the O—O peroxo bond of PMS/PDS via redox mechanism to generate sulfate radicals. Since this bond is highly stable at room temperature, breaking it is only realized when high energy and chemical activators are used [128,132,133]. Some researchers employed heat, ultraviolet irradiation, and ultrasound system as source of energy, whereas chemical activators include sulfides, transitional metal ions and their metal oxides together with their complexes. However, the choice of chemical activators should be investigated properly as they introduce secondary pollution from toxic metal ions. The common utilised precursors for sulfate radicals' generation possess different properties and that lead to difference in activation and catalytic power. The PDS has higher potential (E° ($S_2O_8^{2-}$/$SO_4^{\bullet-}$) = 2.01 V_{NHE}) than PMS (E° (HSO_5^-/$SO_4^{\bullet-}$) = 1.75 V_{NHE}) and its cost is estimated at 0.74 USD/kg (0.18 USD/mol) while 2.2 USD/kg (1.36 USD/mol) is the cost for PMS [134,135]. Furthermore, PDS has a longer O—O peroxo bond distance (1.497 Å) as opposed to PMS (1.460 Å) and this makes it easier to be activated. For the purpose of this review activation of both precursors by Z-scheme photocatalysts will be discussed for degradation of pharmaceutical water pollutants. It should be noted that the higher degradation efficiencies of PMS/PDS based photocatalytic systems emanates from the production of reactive radical ($SO_4^{\bullet-}$, $^{\bullet}OH$, and $^{\bullet}O_2^-$) and non-radical ($^1O_2$) species due to synergistic effect of PDS/PMS and Z-scheme systems. The synergy can be better understood by the description of the processes that are involved during the activation of persulfate with Z-scheme systems. The persulfate can be activated directly by UV radiation to form both sulfate and hydroxyl radicals Eqn. (5) which can degrade pharmaceuticals [136]. The initial step of Z-scheme activation of persulfate is the generation of electrons and holes under light irradiation by the Z-scheme heterostructure. The adjacent persulfate anions accept an electron or hole generated by the Z-scheme system to directly or indirectly transform into sulfate radicals [137]. The general equations involved in the step by step direct or indirect sulfate radicals formation by PMS and PDS normally occur in different mechanisms, and the example using PMS is summarised by Eqn. (6)–(8) [138] while that of PDS is summarised by Eqn. (9)–(10). The sulfate radicals can also generate OH radicals while the superoxide anion radicals can be transformed to sulfate radicals increasing the flux of strong oxidising sulfate and OH radicals. The formed persulfate radicals on the surface of the catalyst, and the catalyst generated radicals results in increased generated radical's flux that synergistically attacks adsorbed pollutants for robust degradation of pollutants. The ability of Z-scheme systems to have continuous generation of electrons enhances the generation of sulfate radicals for better performance as illustrated in Fig. 6a.

$$HSO_5^-/SO_5^{2-} + hv \rightarrow SO_4^{\bullet-} + \cdot OH \quad (5)$$

$$HSO_5^- + e^- \rightarrow SO_4^{\bullet-} + OH^- \quad (6)$$

$$h^+ + HSO_5^- \rightarrow SO_5^{\bullet-} + H^+ \quad (7)$$

$$2SO_5^{\bullet-} \rightarrow 2SO_4^{\bullet-} + O_2 \quad (8)$$

$$S_2O_8^- + e^- \rightarrow SO_4^{\bullet-} + SO_4^{2-} \quad (9)$$

$$S_2O_8^{2-} + \cdot OH \rightarrow S_2O_8^{\bullet-} + OH^- \quad (10)$$

However, the co-existence of sulfate and hydroxyl radicals may decrease the degradation of pharmaceuticals through their reaction that generate a non-radical PMS ($SO_4^{\bullet-}$ + $^{\bullet}OH$ → HSO_5^-) [139].

Ji et al. [132] prepared a perylene diimide (PMI)/MiL-101(Cr) (PMS) Z-scheme heterojunction using one-pot method and used it for activation of PMS under visible light for degradation of iohexol (IOH) drug. The authors achieved degradation efficiency of ~100 % in an illumination time and PMS concentration of 35 min and 3.0 mM, respectively. The IOH degradation mechanism portrayed the production of reactive species for initiation of both radical and non-radical based reactions. Electron spin resonance (ESR) tests (Fig. 6b-c) indicated that participation of Z-scheme was vital as the signals for $SO_4^{\bullet-}$, $^{\bullet}OH$, $^{\bullet}O_2^-$, and singlet oxygen ($^1O_2$) was produced in the presence of visible light. The presence of oxygen containing radicals and holes was also confirmed by scavenger experiments which showed that the holes and $^{\bullet}OH$ were dominant radicals that contributed to effective IOH degradation. The

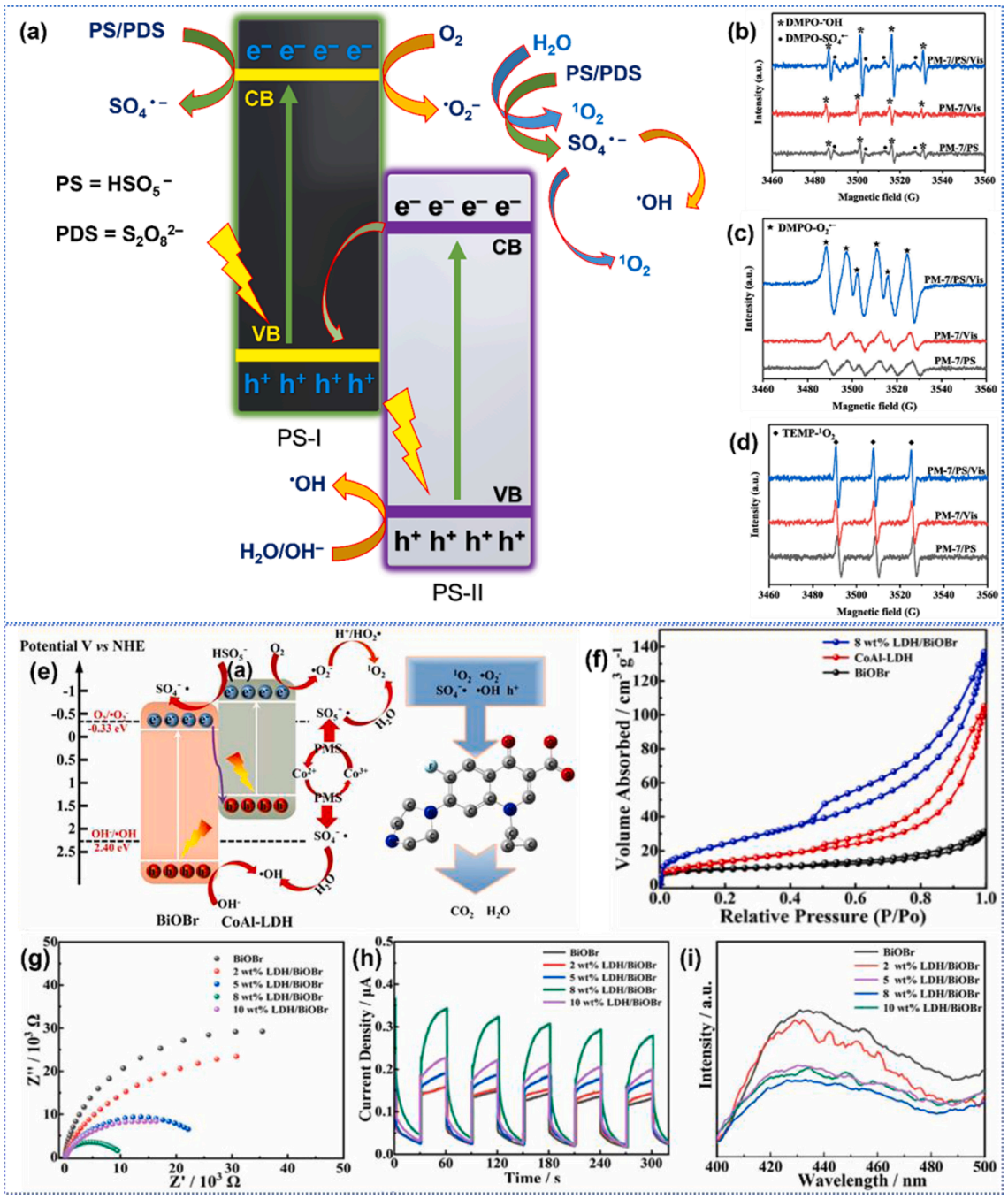

Fig. 6. (a) The general activation of PMS/PDS with Z-scheme heterojunction (excited electrons effect). The EPR signals of (b) DMPO-•OH and DMPO-$SO_4^{\bullet-}$, (c) DMPO-$^{\bullet}O_2^-$ and (d) TEMP-$^1O_2$ in the PM-7/PS, PM-7/Vis and PM-7/PS/Vis systems [132], (e) mechanism of charge generation for CIP degradation in the 8 wt% LDH/BiOBr/PMS/vis system, (f) Nitrogen adsorption–desorption isotherms, (g) EIS plots, (h) Transient photocurrent responses, and (i) PL spectra of BiOBr and its composites [131].

results proved the concept of high charge separation and utilization of visible light irradiation for effective activation of PMS. Likewise, a 2D/2D CoAl-LDH/BiOBr Z-scheme photocatalyst was prepared via hydrothermal method and its application revealed 96 % removal of ciprofloxacin (CIP) on 8 wt% LDH/BiOBr/PMS/Vis system within 30 min at optimum catalyst and PMS doses of 40 and 100 mg, respectively. The CIP degradation was initiated by reactive radicals as shown in Fig. 6e. The authors allied the high CIP elimination to several factors such as strong intimacy interaction between the materials, high specific surface area (91.38 $m^2\ g^{-1}$) which was higher than that of CoAl-LHD (50.80 $m^2\ g^{-1}$), and BiOBr (30.60 $m^2\ g^{-1}$), and enhanced charge carrier separation and migration as demonstrated by EIS, transient photocurrent response and PL results (Fig. 6f-i). The 8 wt% LDH/BiOBr/PMS/Vis system was further extended to TC (98 %), ENR (88 %), NOR (88 %), and RhB (100 %), respectively. It was discussed that the high degradation efficiencies obtained confirmed the synergistic effect between photocatalysis and PMS activation in the LDH/BiOBr/PMS/Vis system. The scavenger and EPR experiments indicated the prevalence of radical ($^{\bullet}O_2^-$) and non-radical ($^1O_2$) degradation of CIP [131]. The synergy between photocatalysis and PMS/PDS activation is the cause of observed short degradation times compared to when only Z-scheme heterojunctions are employed under similar conditions without PMS/PDS oxidants, and the

attained efficiencies of this synergy are normally close to 100 % and accomplishes almost complete mineralisation of organic pollutants in water. Z-scheme mechanism activation of PMS/PDS have been explored by other researchers [127,130,140–144] for pharmaceuticals and other organic pollutant elimination.

Recently, studies have shown that direct Z-scheme heterojunctions are preferred over all solid state/mediator-assisted Z-scheme heterojunctions for activation of PMS/PDS [130,132,141]. The mediator-assisted Z-scheme has been plagued with notable drawbacks such as the cost of noble metals normally used, absorption of photons and electrons by mediators which tend to limit the performance of the process while direct Z-scheme is intimately designed to operate as a sieve for the used photo-electron-hole pairs possessing low redox potential, thus minimising the light shielding effect and uplifting the redox capabilities [135]. The intimate contact in a direct Z-scheme heterojunction also induces formation of electric field which is vital for redox ability needed for redistribution of carrier charges. Afterwards, the Z-scheme photocatalytic system results in more positive valence band and negative conduction band which are vital for both PMS/PDS activation and absorption of more solar light throughout the entire solar spectrum.

4.3. Pathogens inactivation

Numerous micro-organisms or disease-causing pathogens have been determined in surface water making their removal very important. This review focusses on bacteria and virus inactivation only. Viruses have

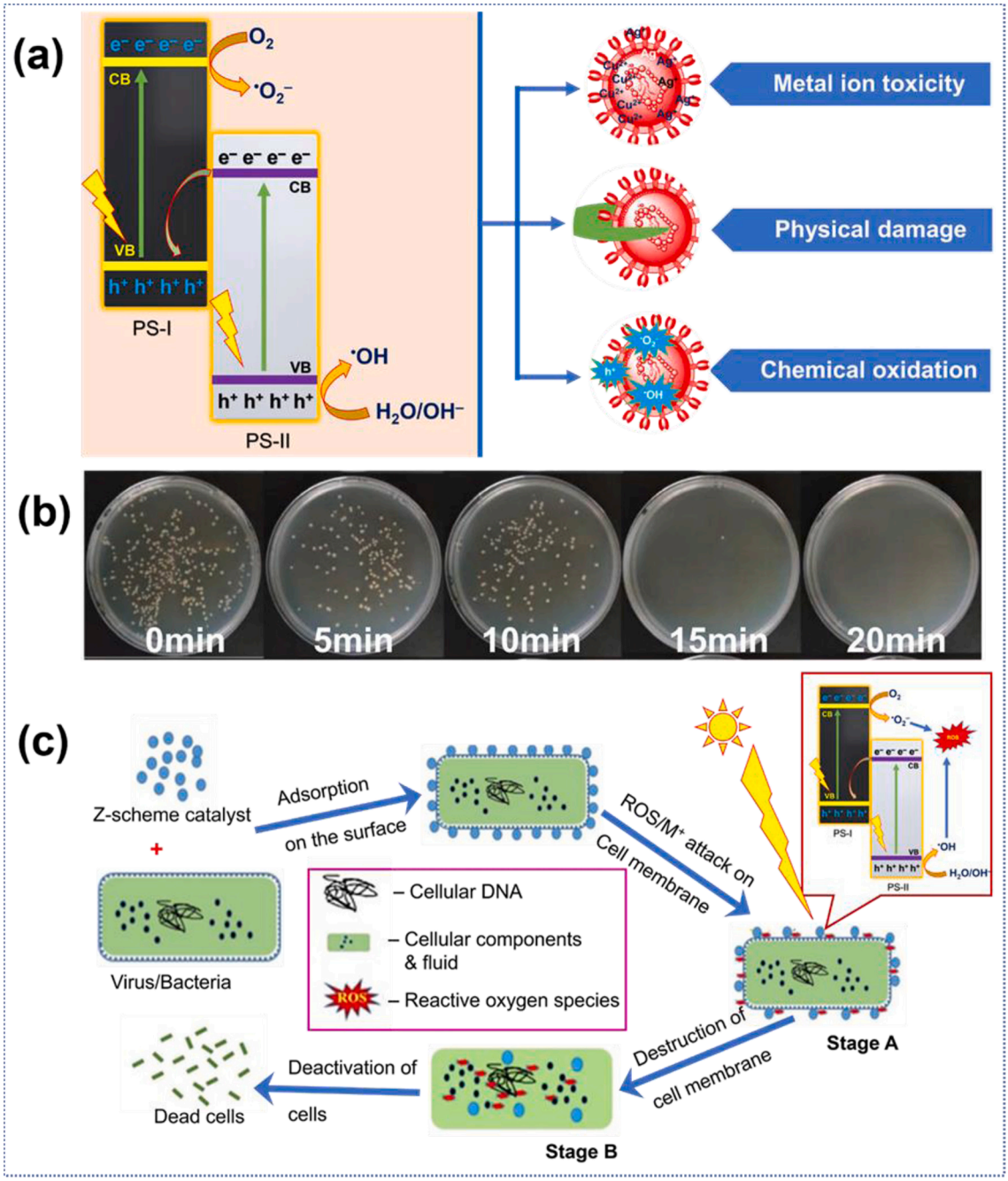

Fig. 7. (a) Three main mechanisms named metal ion toxicity, physical damage, and chemical oxidation for viral/bacterial inactivation induced by Z-scheme heterogeneous photocatalysts (b) photocatalytic antibacterial activity of Z-scheme composite against E. coli at different irradiation times under LED light [45], (c) general schematic presentation of the step by step processes that occur throughout the inactivation process of viruses or bacteria with Z-scheme heterojunctions.

been evaluated directly for their photocatalytic removal with foodborne, airborne and waterborne viruses of supreme prominence [145]. The photocatalytic virus inactivation was first reported on TiO_2 photocatalyst by Sierka and Sjogren in 1994 leading to widespread application of photocatalysis for viral decomposition [146]. The mechanism (like in other pathogen degradation) involves generation of ROS like $^{\bullet}OH$ and H_2O_2 that directly attacks and destroys the virus capsid or cell wall and the cytoplasm releasing contents inside the virus like genetic makeup and proteins [147]. The mechanisms of photocatalytic pathogens inactivation can be subdivided into metal ion toxicity, physical damage and chemical oxidation as suggested by Zhang et al. (Fig. 7a) [1]. In brief, metal ion toxicity hastens inactivation kinetics through synergistic metal ions release and Z-scheme photocatalysis. The metals used in fabrication of Z-scheme systems can be leached into the surface of the pathogens and its synergistic involvement with Z-scheme is the one responsible for heightened virucidal activity. In physical damage, the Z-scheme photocatalyst ROS attack is induced and restricted to the capsid virus protein shells destruction and the contents (Virus RNA, etc.) in the cell leaks out and eventually the pathogen is inactivated after sometime. A chemical oxidation process involves the use of semiconductors under illumination by light of appropriate wavelength for initial generation of electrons and holes which are transformed through redox reactions towards formation of ROSs ($^{\bullet}OH$, h^+, $^1O_2$, H_2O_2, and $^{\bullet}O_2^-$). The generated ROSs attacks the virus membrane and destruct it and continue to completely destruct the contents inside of the membranes to completely inactivate it. It is noteworthy that interaction of catalyst and virus surface, like in photocatalytic pollutant degradation, will enhance efficiency of the processes.

The most commonly studied inactivation of micro-organisms involves bacterial investigations. The antimicrobial evaluation of

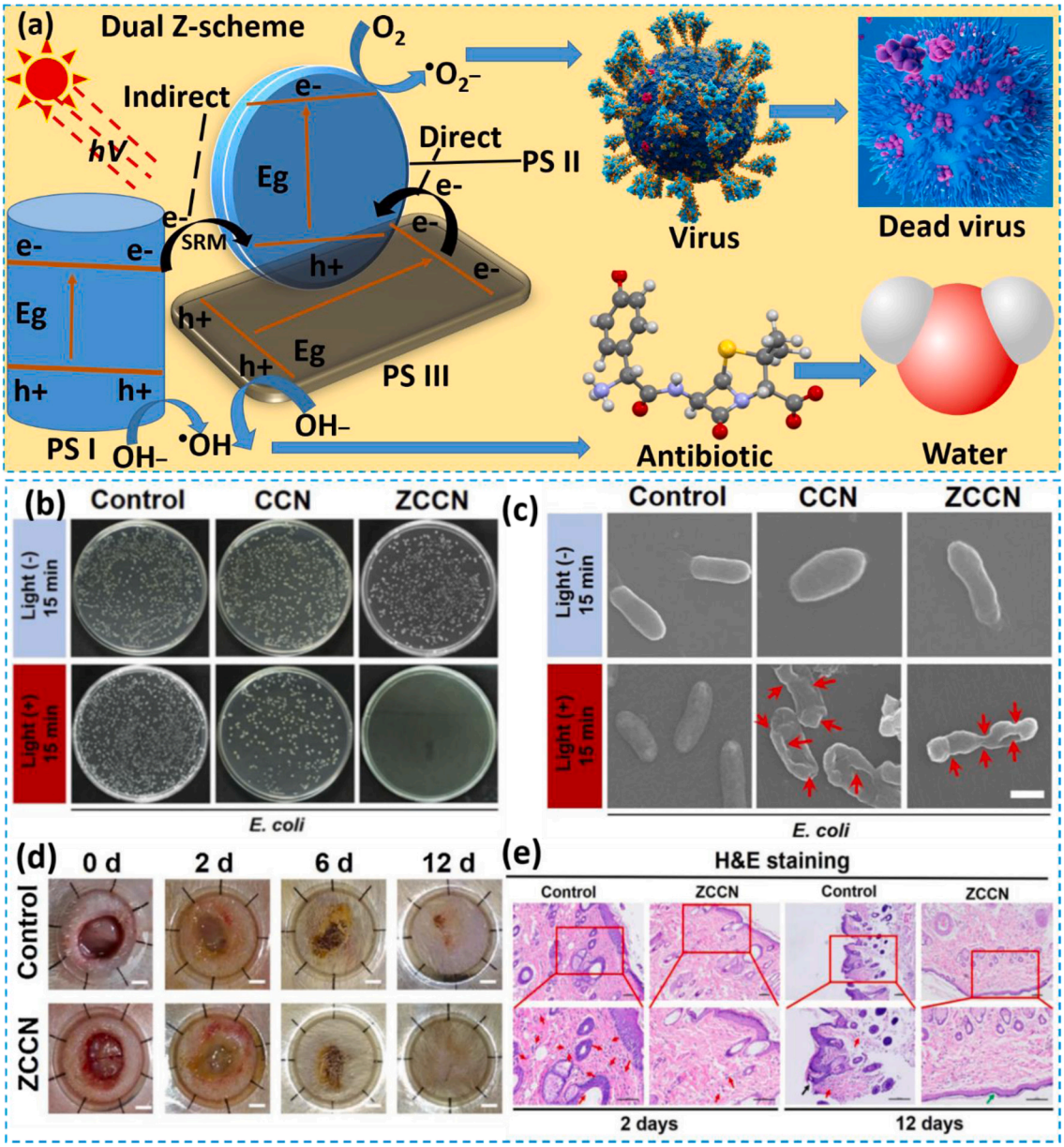

Fig. 8. (a) Indirect, direct and dual Z-scheme presentation for degradation of pharmaceutical (antibiotic) and inactivation of pathogen (virus) (b) Spread plate results of E. coli grown on different samples, (c) Surface morphologies of E. coli treated with different groups with or without 15 min visible light irradiation, scale bars: 1 μm, in vivo assessment of the ZCCN with antibacterial effects and wound healing capability: (d) Photographs of the S. aureus-infected wounds treated with different dressings at time points of 0, 2, 6 and 12 days. Scale bars, 2 mm. and (e) H&E stained images showing the degree of infection of the skin tissue after 2 and 12 days. Scale bars are 50 μm [150].

photocatalytic mechanism involves studies on different bacterial species. Bacterial contamination is a serious concern with numerous bacterial species determined to cause diseases that may result in death from severe diarrhoea making their inactivation a priority in surface and drinking water systems. Liu et al. studied *Escherichia coli* (E. *coli*) and *Staphylococcus aureus* (S. *aureus*) inactivation with direct Z-scheme BiO_{2-x}/BiOBr heterojunction synthesised *in-situ* with oxygen vacancies with bactericidal efficiency of 100 % in 20 min [45]. The increase in irradiation time supervenes decrease in the number of viable bacteria on the culture dish (Fig. 7b). In a recent review by Wang and co-workers [1], different g-C_3N_4 modifications like doping and heterojunction formation were summarised towards photocatalytic inactivation of different classes of bacteria with specific conditions and efficiency highlighted. Xia et al. hydrothermally synthesised a Z-scheme g-C_3N_4/m-Bi_2O_4 towards visible light driven inactivation of 6 log10 cfu/mL of *E. coli* K-12 in 1.5 h [105]. Fluorescence microscopy images after staining with fluorescent dye portrayed an increase of green cells and a decrease in red cells attributed to membrane rapture. SEM images affirmed destruction and distortion of the bacterial structure due to leaking out of important contents resulting in instantaneous inactivation of bacteria by metabolic arrest. Fig. 7c shows a schematic presentation of the step-by-step process that occurs during the inactivation of viruses or bacteria with Z-scheme heterojunctions. Firstly, there should be an interaction between the catalyst and the pathogen, under visible light irradiation, the catalyst attached on the cell wall of bacteria or virus generate ROSs that rapture the cell membrane. The attack leads to destruction of the membrane and the continued release of the ROSs would ensure that contents inside the cell membrane are also destroyed. There are numerous traditional, all solid state and direct Z-scheme heterojunctions associated studies that principally emphasise only bacterial inactivation or bacterial inactivation plus an additional application under visible light irradiation [98,105,148]. The illustration of the charge transfer at the interface during pathogens (virus) direct, indirect, and dual Z-scheme heterojunctions which are similar to pharmaceuticals (antibiotics) degradation to water and carbon-dioxide as shown (Fig. 8a). Indirect Z-scheme comprises the use of an electron mediator as charge transfer route at the interface of the semiconductors to aid recombination of oxidation catalyst CB electrons with VB holes in a reductive semiconductor for enhanced generation of ROSs to initiate bacterial deactivation. In dual Z-scheme, the use of electron mediators may be avoided or collectively used with direct charge transfer with 2 oxidative semiconductors and 1 reductive semiconductor or 2 reductive semiconductors and 1 oxidative semiconductor for enhanced oxidative or reductive performance of the entire Z-scheme system towards antimicrobial performance, respectively.

The popularity of bacterial inactivation with different heterojunctions resulted in fabrication of handy prototypes towards real environmental applications of bacterial inactivation, giving hope for large scale applications of these systems. In medical applications, thermodynamic therapy involves the production of radicals to block electron transport to the tumor cells for energy and nutrients deficiency induced cell death [149]. In wound healing, the ROSs induced by light illumination inhibit bacterial growth resulting in healing of wounds. For example, an indirect Z-scheme ZnO/C-dots/g-C_3N_4 heterojunction fabricated through ultrasonication method was evaluated for wound healing by Xiang et al with antibacterial efficacy of 99.97 % and 99.99 % for S. *aureus* and E. *coli* after 15 min of visible light irradiation, indexed to synergistic contributions of ROSs generation and hyperthermia [150]. In their study, both gram-negative and gram-positive bacteria was selected for visible light driven inactivation on a spread plate method. The results of E. *coli* in 15 min showed no reduction of bacterial count with the control, little reduction with CN and complete removal with a Z-scheme ZnO/C-dots/g-C_3N_4 ternary heterojunction (Fig. 8b). The SEM analysis of the bacteria structure shows more distortion with holes when the Z-scheme ZnO/C-dots/g-C_3N_4 ternary heterojunction was employed compared to no changes and little change for control and CN, respectively (Fig. 8c). In-vivo wound healing was organized with rats wounds (20 mm diameter) infested with 20 μL of S. *aureus* (1×108 CFU/mL) to assess the wound therapeutic ability of the catalyst. The images of the wounds confirmed faster healing in 12 days when the Z-scheme catalyst is used compared to the control experiment after initial S. *aureus* infection after 2 days in both cases (Fig. 8d). Further inspection of the hematoxylin and eosin (H&E) was performed to stain wound tissues. After 2 days, the composite had less inflammatory cells (GRAN, neutrophil granulocyte, red arrows) than the control group, yet after 12 days, necrosis of epidermal cells and epidermal crevices were witnessed in the control group while restoration curative outcome, and unharmed hypodermal tissue arrangement was observed with Z-scheme composite group (Fig. 8e).

The direct degradation of viruses has been studied and it is an emergent area of research with numerous articles focusing on the topic of their possible removal with advanced oxidation processes in water, air and food [147,151–153]. Z-scheme heterojunction inactivation of viruses is no exception, but only a handful of research outputs exist to this regard similarly to Z-scheme remediation of antiviral drugs in water systems. Zhang et al. used a facile solvothermal-hydrothermal method to fabricate a direct Z-scheme heterostructure of oxygen-doped graphitic carbon nitride microspheres (O-g-C_3N_4) and carbonation carbon (HTCC) for visible light inactivation of human adenovirus type 2 (HAdV-2) with virucidal efficiency of $-5\log[C/C_0]$ in 120 min [106]. The increase of temperature to 37 °C further ensued complete removal efficiency at pH 5. The viral particle damage was studied with TEM where after 120 min of irradiation, HAdV-2 structure was ruptured and only virus debris was observed indicating the severity and lethality of the all-organic O-g-C_3N_4/HTCC-2 Z-scheme heterostructure under visible light irradiation. The fabricated nanoparticles cytotoxicity was evaluated through the XTT assay with human A549 cells portraying that within photocatalytic inactivation dosages, the nanoparticles toxicity is negligible with 85 % remaining even at higher concentrations of 150 μg/mL. This validates the biocompatibility and the negligible cytotoxicity indexed to stability and chemical composition of the composites. Cheng and co-workers investigated Ag_3PO_4/g-C_3N_4 heterojunction with Z-scheme charge transfer at the interface synthesised by hydrothermal method towards complete inactivation of bacteriophage f2 with concentration of 3×10^6 PFU/mL under visible light irradiation in 80 min [154]. Scavenger tests were performed to validate charge transfer mechanism of Z-scheme and humic acid retarded the virucidal activity of the composites. As with bacterial inactivation, increase with irradiation time decreased the cultured viral count with none observed after 80 min of irradiation. Numerous investigations into Z-scheme heterojunctions have propelled knowledge broadening proved by recent increase of publications in this regard with numerous novel discoveries like in-situ generation of electron shuttles in direct Z-scheme composites.

The above discussed methods fabricated with the indicated conditions, mechanisms and material configurations can be improved through structural modifications aimed at improving factors that affect pharmaceuticals degradation and pathogens inactivation like the photocatalysts light utilization, enhanced pollutant adsorption and interfacial charge transfer dynamics. Z-scheme heterostructure modifications and fabrication strategies are governed by geometry, morphology variations, or addition of another material for synergy [6,155,156]. The universal method that is employed as an improvement mechanism to Z-scheme systems performance is the directed modulation of its morphology. The alterations of morphology can significantly boost photodegradation efficiency of catalysts for pharmaceuticals degradation by reduction of the diffusion length of charge carriers. The variations of photocatalytic composites formation conditions (use of different methods) results in changes in morphology that can be targeted based on semiconductor properties. The modification of semiconductors band structure with doping, generation of defects or molecular grafting is another important materials modulation strategy that assists with increasing the efficient charge transportation [156,157]. With vacancies as an example, charge

transfer efficiency between PS I and PS II interface will be enhanced by generated defects such as oxygen vacancies, sulfur vacancies or dopant-induced interfacial defects to augment the interfacial charge transfer (Fig. 9a). The induced defects (especially oxygen defects) increases the light harvesting ability of the photocatalyst composite, enhance interfacial charge separation, and increase available reaction sites for photocatalytic reactions.

The effect of coupling surface plasmon resonance materials (SPR) applied mainly to Z-scheme systems is a promising strategy (Fig. 9b). The semiconductor and SPR material synergy is reflected by superior

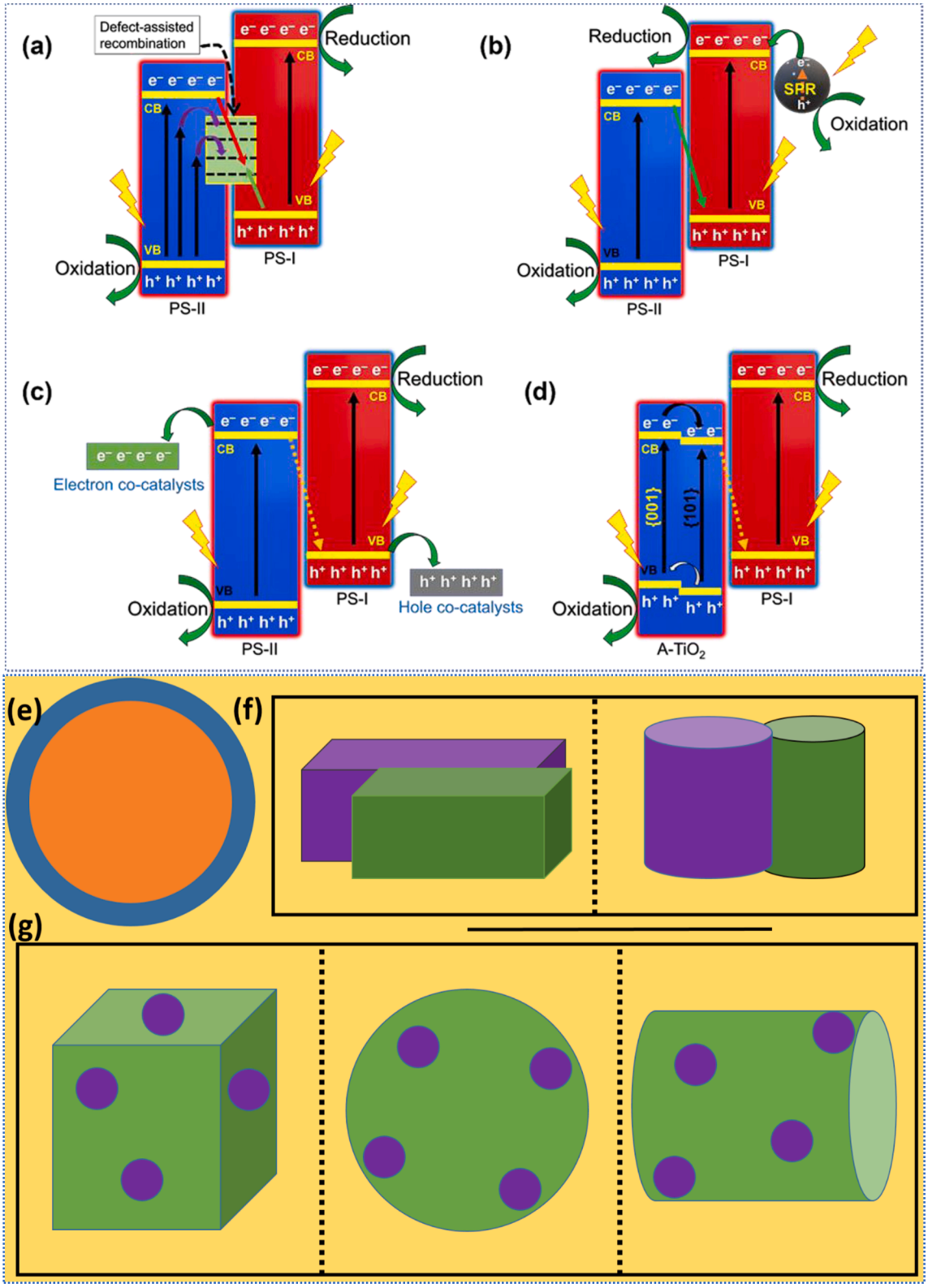

Fig. 9. Improvement of Z-scheme systems with (a) defect-assisted charge transfer, (b) surface plasmon resonance material, (c) holes and electrons co-catalysts, (d) facet engineered charge transfer, (e) core–shell structure, (f) Janus-type geometry, and (g) surface decorated artichectures.

light harvesting ability of the Z-scheme system in visible or NIR region of the solar spectrum and SPR-induced electromagnetic fields that can enhance charge separation at the semiconductor and SPR interfaces [35]. The SPR that are commonly used are noble metals [56]. The development of full solar spectrum (UV–vis-NIR) active photocatalytic systems is another interesting strategy that employs 100 % light source from the solar spectrum when non-linear up-conversion photoluminescence (UCPL) materials are integrated into Z-scheme systems [35]. Co-catalysts can be introduced to Z-scheme heterojunctions for effective suppression of photogenerated electron and hole pairs (Fig. 9c). This increases photocatalytic activity through reduction of some reactions activation energy and improves the charge transfer for recombination of useless electrons in the conduction band of the oxidative semiconductor and useless holes in the valence band of the reductive semiconductor with specific co-catalysts classified as electron co-catalysts and holes co-catalysts for electron or hole capturing semiconductors, respectively. Co-catalysts examples include carbon materials (rGO), noble metals (Pd, Pt), and some semiconductors (CeO_2, ZnO, etc.) [28]. This could further be described as cascade dual Z-scheme heterostructure when one semiconductor is used as both electrons and holes co-catalyst [158]. Another fabrication strategy that has been determined to increase photocatalytic performance efficiency of Z-scheme heterostructures include facet engineering. The different surface energies possessed by different crystalline facets of a single semiconductor can be tailored to enhance certain properties of Z-scheme heterojunctions. This property has been employed to channel charge transportation route and direction between Z-scheme semiconductor interfaces [35]. The most common example of this fabrication strategy with anatase TiO_2 co-exposed {1 0 1} and {0 0 1} facets as an oxidative semiconductor and reductive (PS I) semiconductor generates a Z-scheme charge transfer at the interface of {1 0 1} anatase TiO_2 exposed facets and PS I (Fig. 9d). Inter-semiconductor heterojunction will form when electrons transfer from {0 0 1) to {1 0 1} and holes transfer from {1 0 1} to {0 0 1} exposed facets of TiO_2. The incorporation of a PS I to {1 0 1} anatase TiO_2 exposed facets induces charge transfer from electron donor {1 0 1} facet to PS I valence hand to react with its holes resulting in Z-scheme mechanism. The geometry modulation has been employed for the degradation of pollutants with Z-scheme catalysts with Janus-type, core–shell, and surface decorated architectures commonly employed. Core-shell involves the complete coverage of a semiconductor to be a core of another catalyst with the size of the outer layer important to allow passage of light to the inner semiconductor to induce excited electrons and holes pairs (Fig. 9e). Janus type heterostructures can be varied into spherical or any similar shaped semiconductors attached parallel to one another (Fig. 9f). Surface functionalization may be applied for strong interaction of the semiconductors at the interface for improved charge transfer efficiency. Surface decorated systems strategic fabrication is governed by decorating the surface of one semiconductor with another with similar or different semiconductor shapes uniformly or non-homogeneously distributed (Fig. 9g) [159]. The fabrication strategies have been largely employed for direct Z-scheme heterojunctions due to their high comparative degradation activity for pathogen inactivation and pharmaceutical pollutants remediation compared to indirect Z-scheme heterojunctions.

5. Advancements in Z-scheme photocatalysts

5.1. Evolution of S-scheme

After numerous investigations of the direct Z-scheme, another mechanism referred to as the S-scheme was introduced in 2019 by Fu et al [160]. There is no difference in the reported S-scheme mechanism (Fig. 10a) and the direct Z-scheme (Fig. 10b) based on materials and thermodynamic perspectives, and the pre-requisite conditions are the same with the same properties at the interfaces that results in their formation as evident from already reported S-scheme heterojunctions

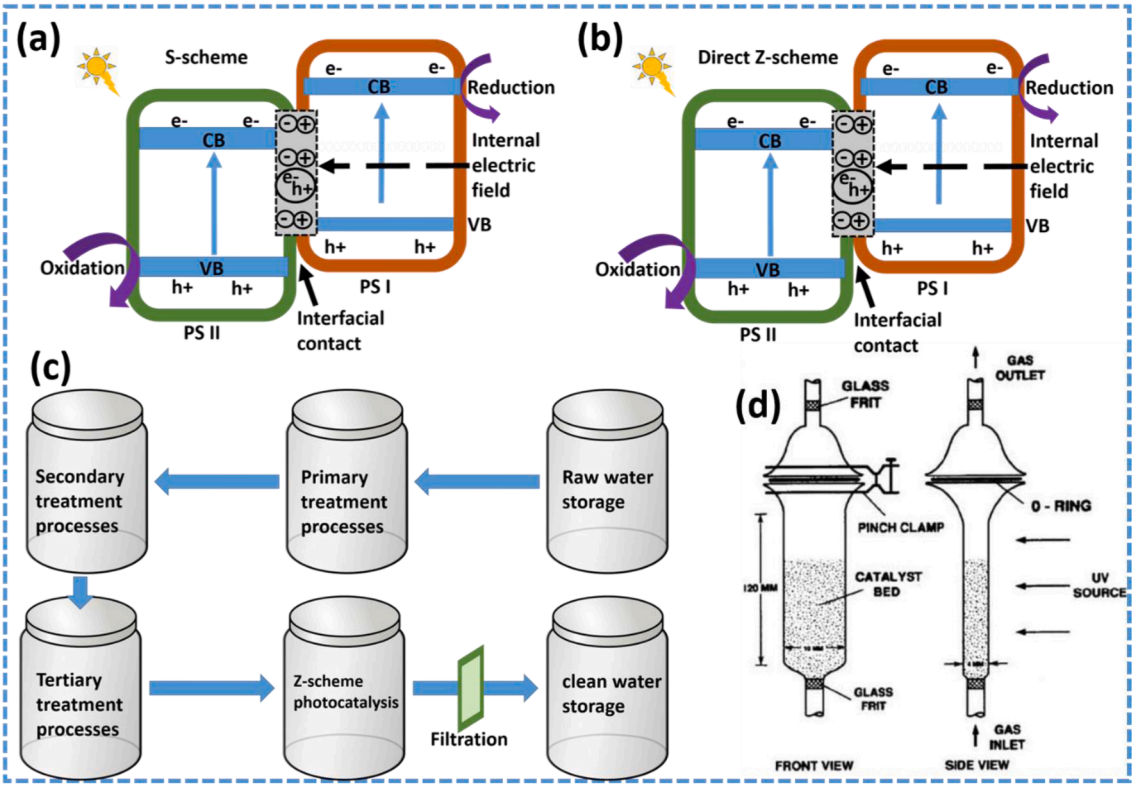

Fig. 10. (a, b) Examples of similar S-scheme mechanism and direct Z-scheme charge transfer heterostructures, (c) envisaged appropriate Z-scheme photoreactor installation position in a conventional wastewater treatment plant, and (d) Schematic diagram of a PCO fluidized bed reactor [169].

[61,110,123] in comparison with some direct Z-scheme heterostructures [113,161,162]. For example, as correctly pointed out by Liao and co-workers in their review based on Z-scheme catalytic systems, both S-scheme and direct Z-scheme mechanisms require a unique principle of high work function of oxidative semiconductor (PS II) compared to that of the reductive semiconductor (PS I) [163]. The build-in electric field is reported as the only means of interface charge recombination driving force in Z-scheme while coulomb attraction and bend bending also act as driving forces for interface recombination of charges in S-scheme system. Equivocally, some reports on Z-scheme mechanisms exist with Xu et al. reporting band bending induced by In-O-Cd bond as a driving force for interface charge recombination enhancement in $ZnIn_2S_4$/CdS material fabricated via cation exchange reaction towards efficient photoelectrochemical water splitting [164]. Therefore, the coulomb force, band bending and internal-build in electric field contribution for recombination of electrons and holes at the interface of semiconductors can be considered a good discovery for enhancement of knowledge and understanding in direct Z-scheme heterostructures. A strong recommendation is made that the word S-scheme can be regarded as another name for direct Z-scheme heterojunction by scientific community. It is reported that the S-scheme comprises mainly of two *n*-type photocatalysts in which one is oxidation photocatalyst and another reduction photocatalyst. The migration and movement of electrons follows a "step" (macroscopic viewpoint) or "N" (microscopic viewpoint) type for effective separation of carrier charges [34]. However, this kind of heterojunction is at its infancy stage and need to be explored more in the future and all-encompassing assessment with analogous scientific procedures maybe directed to determine a reasonable alteration with direct Z-scheme systems to evade confusion and misconception of forthcoming works.

5.2. Laboratory Up-scaling

The possible applicability of Z-scheme photocatalytic heterojunctions for real wastewater applications needs laboratory validations mimicking real wastewater compositions for proper analysis of actual expected behavioural activities and the minimum required time towards achieving meaningful efficiencies. In this regard, Wang et al. used a hydrothermal method to synthesise a 0D/2D/2D $ZnFe_2O_4$/$Bi_2O_2CO_3$/BiOBr double Z-scheme heterojunctions for visible light degradation of three tetracycline antibiotics like tetracycline (TC), oxytetracycline (OTC), and doxycycline (DOX) with 93 %, 90.1 %, and 89.4 % degradation efficiencies under sunlight and PMS system for 20 min [115]. Direct double Z-scheme mechanism was established with quenching experiments, DFT calculations, EPR measurements, and XPS valence band spectra with two oxidative semiconductors ($Bi_2O_2CO_3$ and BiOBr) and one reductive semiconductor ($ZnFe_2O_4$) forming an arrow-up heterojunction. From this study, despite the analysis of the effects of different anions, the analysis of different secondary effluents from a sewage treatment plant were used to prepare 20 ppm solutions of TC OTC, and DOX with 85.6 %, 82.8 %, and 82.5 % degradation efficiencies in 20 min, respectively. The small decrease of less than 10 % gave extraordinary confidence towards real wastewater applications with oxidants (PMS) enhanced dual Z-scheme photocatalytic systems in real wastewater matrixes for remediation of pharmaceuticals in polluted water.

Different reactor designs have been investigated to address the challenge of expensive filters required to dodge nanomaterials discharges into the environment. This dispersion which results in high quantum efficiency due to good pollutant and catalyst interaction is common despite causing secondary pollution [165]. The widely employed fluidized bed reactor contains a system for easy recovery of catalysts after application. However, if utilized for industrial, commercial, and domestic wastewater treatment plants, it should be integrated into the conventional plants as a tertiary treatment process following other tertiary processes like filtration and followed by discovery methods to reduce nanomaterials route into clean water which may leak into the solution from the fixed bed reactor (Fig. 10c). This reactor-type can allow batch and continuous modes of operation but necessary retention time will be required for pollutant degradation process in both systems with more time required in the former than the latter. The fluidized-bed photoreactors are designed such that the light source can either be tubular UV lams or LED lights placed at the centre, externally or wrapping the interior of the reactor walls with a barrier between them and the solution (Fig. 10d). The reviews on Z-scheme photocatalysis for degradation of pollutants do not have a discussion on possible application of Z-scheme photocatalytic reactors at pilot scale [91,166]. Therefore, it is important to analyse this aspect with a view to encourage more studies to be tailored towards pilot scale testing of Z-scheme heterojunctions towards water pollution remediation for drinking water security and safety. Most reported Z-scheme photoreactors have been reported towards water splitting for HER and OER. Chandran et al. [167] assessed a micro-scale photocatalyst suspension in aqueous solution with a traditional Z-scheme charge transfer mechanism on a tandem particle-suspension reactor design for solar water splitting. Expedition of redox species conveyance between hydrogen and oxygen evolution reaction compartments to forfeit gas crossover is achieved through a porous separator while its superior performance is attributed to proton-coupled electron mediators (*para*-benzoquinone/ hydroquinone and iodide/iodate) with zero visible light absorption capacity. A 1 cm high reaction stall containing 2.2 mg of $BiVO_4$ and $SrTiO_3$: Rh particles was predicted to sustain reactor operational efficiency at 1 % with fast diffusive species transportation. Su et al. designed a mediator free Z-scheme twin reactor for isolated HER and OER during photocatalytic water splitting reaction [168]. A single Nafion membrane divided reactor was segmented into two distinctive chambers of $CuFeO_2$ and $Bi_{20}TiO_{32}$ as HER and OER powder catalysts, respectively. Reduced graphene oxides were used as electron mediators with branched copper wires employed to further enhance the electron collection in a Z-scheme interfacial charge transfer mechanism for water splitting. HER and OER efficiency was 2.23 and 1.14 in this reactor showing a stoichiometric ration of 2:1 with advantages such as hydrogen purification cost avoidance, and avoidance of potential explosion. It was suggested that the system can potentially be employed for wider range of applications like water pollution remediation. However, alarming scarcity of industrial systems in water purification sums up the lack of interest and trust from investors and thus limiting research aimed at large scale application of Z-scheme heterostructures and advanced oxidation processes in general.

6. Conclusion and perspectives

With the current Covid-19 pandemic inducing muddle amongst scientists and the public, the time to exercise the supremacy of scientific technology in unravelling tangible and current problems on a global scale is now. Z-scheme photocatalysts posture high charge separation efficiency with separate PS I and PS II ensuring strong redox ability making them more efficient than other heterojunctions. The addition of oxidants like PMS/PDS have been established to heighten catalytic performance while reactor design is envisaged as an essential aspect towards industrialization of Z-scheme photocatalytic composites for water treatment. Despite tremendous work and discoveries associated with Z-scheme photocatalytic applications in pharmaceuticals degradation and pathogens inactivation, lack of practical competency appeals for imminent considerations.

Z-scheme photocatalytic degradation of pharmaceuticals or inactivation of pathogens should be explored largely with profuse sunlight energy with appropriate reactors designed and optimised for this purpose using experimental findings and modelling techniques such as DFT for efficient performance. This requires careful selection of oxidative and reductive semiconductors with strong visible light absorption index, optimised charge transfer at the interface of the semiconductors with an

in-depth study of more than one technique to complementarily prove Z-scheme mechanism existence, ease separation of the photocatalytic materials from the treated water with options like use of supports, magnets, etc., evaluation and assurance of the photocatalytic composites safety to human health and proper evaluation of their permissible limits in the water environment, and optimization of fabricated prototypes for economic viability, readiness of investors into this new technology, and its possible integration into existing wastewater treatment technologies for low installation, operation and maintenance costs. The recent reports on S-scheme heterojunctions needs to be explored in detail to reach a scientific consensus with evidence of their difference with direct Z-scheme heterojunctions.

Considering the multitudes of investigations performed on elimination of bacteria with Z-scheme heterostructured composites, it is imperative that more work needs to be done to completely understand the mechanism of their destruction with systematic evaluations of the fate of the contents inside the membranes after destruction of the cell wall. Furthermore, the lack of evaluations of Z-scheme heterostructures for viral inactivation is alarming, and considering the current Covid-19, more work needs to be pioneered towards laboratory scale investigations of SARS-CoV-1, MERS-CoV and Covid-19 virucidal activities of Z-scheme charge transfer composites. Lastly, the applications of external oxidants like PMS/PDS, hydrogen peroxide, and ozone should be explored with Z-scheme photocatalytic composites as viral disinfection materials in water systems with explorations of near real environmental compositions as they are appeasing photocatalytic performance enhancers. PMS/PDS have been determined to be activated by UV light only which will ensure non-selective synergistic activity for destruction of pathogens and pharmaceuticals in water when employed concurrently with Z-scheme systems. There is a need for out-of-the-box solutions that will encompass high interfacial charge transfer, 100 % solar irradiation spectral activation, and high stability photocatalytic materials for real environmental applications in water pollution remediation.

The issues above can be considered both challenges and opportunities to environmental, materials and chemical engineers, investors, and researchers in water disinfection and photocatalysis fields. The onus of this work is to stimulate knowledge in Z-scheme photocatalytic materials, draw more attention to researchers and investors in this field, and encourage its large-scale applicability to solve current problems for socio-economic sustainability and development.

CRediT authorship contribution statement

Mope Edwin Malefane: Conceptualization, Methodology, Writing – original draft. **Potlako John Mafa:** Writing – original draft, Methodology. **Thabo Thokozani Innocent Nkambule:** Writing – review & editing. **Muthumuni Elizabeth Managa:** Writing – review & editing. **Alex Tawanda Kuvarega:** Writing – review & editing, Supervision, Funding acquisition.

Declaration of Competing Interest

The authors declare that they have no known competing financial interests or personal relationships that could have appeared to influence the work reported in this paper.

Data availability

No data was used for the research described in the article.

Acknowledgements

This work was financially supported by Institute for Nanotechnology and Water Sustainability (iNanoWS) at UNISA and the National research Foundation (NRF) (Grant number: 129282).

Appendix A. Supplementary data

Supplementary data to this article can be found online at https://doi.org/10.1016/j.cej.2022.138894.

References

[1] W. Wang, C. Zhou, Y. Yang, G. Zeng, C. Zhang, Y. Zhou, J. Yang, D. Huang, H. Wang, W. Xiong, X. Li, Y. Fu, Z. Wang, Q. He, M. Jia, H. Luo, Carbon nitride based photocatalysts for solar photocatalytic disinfection, can we go further? Chem. Eng. J. 404 (2021), 126540 https://doi.org/10.1016/j.cej.2020.126540.
[2] R. Cao, H. Yang, S. Zhang, X. Xu, Engineering of Z-scheme 2D/3D architectures with Ni(OH)2 on 3D porous g- C3N4 for efficiently photocatalytic H2 evolution, Appl. Catal. B Environ. 258 (2019), 117997, https://doi.org/10.1016/j.apcatb.2019.117997.
[3] D. Huang, S. Chen, G. Zeng, X. Gong, C. Zhou, M. Cheng, W. Xue, X. Yan, J. Li, Artificial Z-scheme photocatalytic system: What have been done and where to go? Coord. Chem. Rev. 385 (2019) 44–80, https://doi.org/10.1016/j.ccr.2018.12.013.
[4] L. Xie, T. Du, J. Wang, Y. Ma, Y. Ni, Z. Liu, L. Zhang, C. Yang, J. Wang, Recent advances on heterojunction-based photocatalysts for the degradation of persistent organic pollutants, Chem. Eng. J. 426 (2021), 130617, https://doi.org/10.1016/j.cej.2021.130617.
[5] M.E. Malefane, Photocatalytic nanocomposites for degradation of organic pollutants in water under visible light, University of South Africa, 2019.
[6] Q. Xu, L. Zhang, J. Yu, S. Wageh, A.A. Al-ghamdi, M. Jaroniec, Direct Z-scheme photocatalysts: Principles, synthesis, and applications, Mater. Today. 21 (2018) 1042–1063, https://doi.org/10.1016/j.mattod.2018.04.008.
[7] Y. Bao, S. Song, G. Yao, S. Jiang, S-Scheme Photocatalytic Systems, Sol. RRL. 5 (2021) 2100118, https://doi.org/10.1002/solr.202100118.
[8] T. Di, Q. Xu, W. Ho, H. Tang, Q. Xiang, J. Yu, Review on Metal Sulphide-based Z-scheme Photocatalysts, ChemCatChem. 11 (2019) 1394–1411, https://doi.org/10.1002/cctc.201802024.
[9] K. Wang, Y. Li, G. Zhang, J. Li, X. Wu, 0D Bi nanodots/2D Bi3NbO7 nanosheets heterojunctions for efficient visible light photocatalytic degradation of antibiotics: Enhanced molecular oxygen activation and mechanism insight, Appl. Catal. B Environ. 240 (2019) 39–49, https://doi.org/10.1016/j.apcatb.2018.08.063.
[10] Y. Jiang, K. Huang, W. Ling, X. Wei, Y. Wang, J. Wang, Investigation of the kinetics and reaction mechanism for photodegradation tetracycline antibiotics over sulfur-doped Bi2WO6-x/ZnIn2S4 Direct Z-scheme heterojunction, Nanomaterials. 11 (2021) 2123, https://doi.org/10.3390/nano11082123.
[11] G. Lee, H. Chen, J.J. Wu, (In, Cu) Co-doped ZnS nanoparticles for photoelectrochemical hydrogen production, Int. J. Hydrogen Energy. 44 (2019) 110–117, https://doi.org/10.1016/j.ijhydene.2018.02.112.
[12] M.E. Malefane, U. Feleni, A.T. Kuvarega, A tetraphenylporphyrin/WO3/exfoliated graphite nanocomposite for the photocatalytic degradation of an acid dye under visible light irradiation, New J. Chem. 43 (2019) 11348–11362, https://doi.org/10.1039/c9nj02747e.
[13] H. Yang, A short review on heterojunction photocatalysts: Carrier transfer behavior and photocatalytic mechanisms, Mater. Res. Bull. 142 (2021), 111406, https://doi.org/10.1016/j.materresbull.2021.111406.
[14] M.E. Malefane, U. Feleni, A.T. Kuvarega, Cobalt (II/III) oxide and tungsten (VI) oxide p-n heterojunction photocatalyst for photodegradation of diclofenac sodium under visible light, J. Environ. Chem. Eng. 8 (2) (2020) 103560.
[15] J. Chen, C. Hu, Z. Deng, X. Gong, Y. Su, Q. Yang, J. Zhong, J. Li, R. Duan, Insight into visible light-driven photocatalytic performance of direct Z- scheme Bi2WO6/BiOI composites constructed in -situ, Chem. Phys. Lett. 716 (2019) 134–141, https://doi.org/10.1016/j.cplett.2018.12.026.
[16] S. Poirier-larabie, P.A. Segura, C. Gagnon, Degradation of the pharmaceuticals diclofenac and sulfamethoxazole and their transformation products under controlled environmental conditions, Sci. Total Environ. 557–558 (2016) 257–267, https://doi.org/10.1016/j.scitotenv.2016.03.057.
[17] L. Feng, E.D. Van Hullebusch, M.A. Rodrigo, G. Esposito, M.A. Oturan, Removal of residual anti-inflammatory and analgesic pharmaceuticals from aqueous systems by electrochemical advanced oxidation processes. A review, Chem. Eng. J. 228 (2013) 944–964, https://doi.org/10.1016/j.cej.2013.05.061.
[18] X. Wen, Q. Lu, X. Lv, J. Sun, J. Guo, Z. Fei, C. Niu, Photocatalytic degradation of sulfamethazine using a direct Z-Scheme AgI/Bi4V2O11 photocatalyst: Mineralization activity, degradation pathways and promoted charge separation mechanism, J. Hazard. Mater. 385 (2020), 121508, https://doi.org/10.1016/j.jhazmat.2019.121508.
[19] H. Lu, Q. Hao, T. Chen, L. Zhang, D. Chen, C. Ma, W. Yao, Y. Zhu, A high-performance Bi2O3/Bi2SiO5 p-n heterojunction photocatalyst induced by phase transition of Bi2O3, Appl. Catal. B Environ. 237 (2018) 59–67, https://doi.org/10.1016/j.apcatb.2018.05.069.
[20] N. Zhu, C. Li, L. Bu, C. Tang, S. Wang, P. Duan, L. Yao, J. Tang, D.D. Dionysiou, Y. Wu, Bismuth impregnated biochar for efficient estrone degradation: the synergistic effect between biochar and Bi/Bi2O3 for a high photocatalytic performance, J. Hazard. Mater. 384 (2020) 121258.
[21] M.E. Malefane, Co3O4/Bi4O5I2/Bi5O7I C - Scheme Heterojunction for Degradation of Organic Pollutants by Light-Emitting Diode Irradiation, ACS Omega. 5 (2020) 26829–26844, https://doi.org/10.1021/acsomega.0c03881.

[22] B. Chen, L. Zhou, Y. Tian, J. Yu, J. Lie, L. Wang, Y. Liu, J. Zhang, Z-scheme inverse opal CN/BiOBr photocatalysts for highly efficient degradation of antibiotics, Phys. Chem. Chem. Phys. 21 (2019) 12818–12825, https://doi.org/10.1039/c9cp01495k.

[23] X. Li, J. Xia, W. Zhu, J. Di, B. Wang, S. Yin, Z. Chen, H. Li, Facile synthesis of few-layered MoS2 modified BiOI with enhanced visible-light photocatalytic activity, Colloids Surfaces A Physicochem. Eng. Asp. 511 (2016) 1–7, https://doi.org/10.1016/j.colsurfa.2016.09.033.

[24] Y. Chen, G. Zhu, M. Hojamberdiev, J. Gao, R. Zhu, C. Wang, X. Wei, P. Liu, Three-dimensional Ag2O/Bi5O7I p–n heterojunction photocatalyst harnessing UV–vis–NIR broad spectrum for photodegradation of organic pollutants, J. Hazard. Mater. 344 (2018) 42–54, https://doi.org/10.1016/j.jhazmat.2017.10.015.

[25] K. Qi, B. Cheng, J. Yu, W. Ho, A review on TiO2-based Z-scheme photocatalysts, Chinese, J. Catal. 38 (2017) 1936–1955, https://doi.org/10.1016/S1872-2067(17)62962-0.

[26] A. Hassani, S. Krishnan, J. Scaria, P. Eghbali, P.V. Nidheesh, Z-scheme photocatalysts for visible-light-driven pollutants degradation: A review on recent advancements, Curr. Opin. Solid State Mater. Sci. 25 (5) (2021) 100941.

[27] Y. Wang, H. Suzuki, J. Xie, O. Tomita, D.J. Martin, M. Higashi, D. Kong, R. Abe, J. Tang, Mimicking natural photosynthesis: solar to renewable h2 fuel synthesis by Z-scheme water splitting systems, Chem. Rev. 118 (2018) 5201–5241, https://doi.org/10.1021/acs.chemrev.7b00286.

[28] A. Kumar, P. Raizada, P. Singh, R.V. Saini, A.K. Saini, A. Hosseini-bandegharaei, Perspective and status of polymeric graphitic carbon nitride based Z-scheme photocatalytic systems for sustainable photocatalytic water purification, Chem. Eng. J. 391 (2020), 123496, https://doi.org/10.1016/j.cej.2019.123496.

[29] M. Ren, J. Chen, P. Wang, J. Hou, J. Qian, C. Wang, Y. Ao, Construction of silver iodide/silver/bismuth tantalate Z-scheme photocatalyst for effective visible light degradation of organic pollutants, J. Colloid Interface Sci. 532 (2018) 190–200, https://doi.org/10.1016/j.jcis.2018.07.141.

[30] J. Xu, J. Chen, Y. Ao, P. Wang, 0D/1D AgI/MoO3 Z-scheme heterojunction photocatalyst: Highly efficient visible-light-driven photocatalyst for sulfamethoxazole degradation, Chinese Chem. Lett. 32 (2021) 3226–3230, https://doi.org/10.1016/j.cclet.2021.04.003.

[31] S. Patnaik, G. Swain, K.M. Parida, Highly efficient charge transfer through a double Z-scheme mechanism by a Cu-promoted MoO3/g-C3N4 hybrid nanocomposite with superior electrochemical and photocatalytic performance, Nanoscale. 10 (2018) 5950–5964, https://doi.org/10.1039/c7nr09049h.

[32] X. Zhang, X. Wang, J. Chai, S. Xue, R. Wang, L. Jiang, J. Wang, Z. Zhang, D. D. Dionysiou, Construction of novel symmetric double Z-scheme BiFeO3/CuBi2O4/BaTiO3 photocatalyst with enhanced solar-light-driven photocatalytic performance for degradation of norfloxacin, Appl. Catal. B Environ. 272 (2020), 119017, https://doi.org/10.1016/j.apcatb.2020.119017.

[33] W. Xue, D. Huang, X. Wen, S. Chen, M. Cheng, R. Deng, B. Li, Y. Yang, X. Liu, Silver-based semiconductor Z-scheme photocatalytic systems for environmental purification, J. Hazard. Mater. 390 (2020), 122128, https://doi.org/10.1016/j.jhazmat.2020.122128.

[34] Q. Xu, L. Zhang, B. Cheng, J. Fan, J. Yu, S-scheme heterojunction photocatalyst, Chem. 6 (2020) 1543–1559, https://doi.org/10.1016/j.chempr.2020.06.010.

[35] X. Li, C. Garlisi, Q. Guan, S. Anwer, K. Al-ali, G. Palmisano, L. Zheng, A review of material aspects in developing direct Z-scheme photocatalysts, Mater. Today. 47 (2021) 75–107, https://doi.org/10.1016/j.mattod.2021.02.017.

[36] R. Hill, FAY Bendall, Crystallization of a photosynthetic reductase from a green plant, Nature. 187 (4735) (1960) 417.

[37] S. Malkin, Theoretical analysis of the enhancement effect in photosynthesis, Biophys. J. 7 (1967) 629–649, https://doi.org/10.1016/S0006-3495(67)86613-X.

[38] J. Low, C. Jiang, B. Cheng, S. Wageh, A.A. Al-ghamdi, J. Yu, A Review of Direct Z-Scheme Photocatalysts, Small Methods. 1 (2017) 1700080, https://doi.org/10.1002/smtd.201700080.

[39] D. Liu, S. Chen, R. Li, T. Peng, Review of Z-scheme heterojunctions for photocatalytic energy conversion, Acta Phys. 37 (2021) 2010017, https://doi.org/10.3866/PKU.WHXB202010017.

[40] H. Tada, T. Mitsui, T. Kiyonaga, T. Akita, K. Tanaka, All-solid-state Z-scheme in CdS–Au–TiO2 three-component nanojunction system, Nat. Mater. 5 (2006) 782–786, https://doi.org/10.1038/nmat1734.

[41] C. Du, S. Nie, C. Zhang, T. Wang, S. Wang, J. Zhang, C. Yu, Z. Lu, S. Dong, J. Feng, H. Liu, J. Sun, Dual-functional Z-scheme CdSe/ Se/BiOBr photocatalyst: Generation of hydrogen peroxide and efficient degradation of ciprofloxacin, J. Colloid Interface Sci. 606 (2022) 1715–1728, https://doi.org/10.1016/j.jcis.2021.08.152.

[42] G. Gebreslassie, P. Bharali, U. Chandra, A. Sergawie, P.K. Boruah, M.R. Das, A. Esayas, Novel g-C3N4/graphene/NiFe2O4 nanocomposites as magnetically separable visible light driven photocatalysts, J. Photochem. Photobiol. A Chem. 382 (2019), 111960, https://doi.org/10.1016/j.jphotochem.2019.111960.

[43] D. Kilic, M. Sevim, Z. Eroglu, Ö. Metin, S. Karaca, Strontium oxide modified mesoporous graphitic carbon nitride/titanium dioxide nanocomposites (SrO-mpg-CN/TiO2) as efficient heterojunction photocatalysts for the degradation of tetracycline in water, Adv. Powder Technol. 32 (2021) 2743–2757, https://doi.org/10.1016/j.apt.2021.05.043.

[44] X. Wang, G. Liu, Z.G. Chen, F. Li, L. Wang, G.Q. Lu, H.M. Cheng, Enhanced photocatalytic hydrogen evolution by prolonging the lifetime of carriers in ZnO/CdS heterostructures, Chem. Commun. 23 (2009) 3452–3454, https://doi.org/10.1039/b904668b.

[45] J. Liu, L. Huang, Y. Li, L. Yang, C. Wang, J. Liu, Y. Song, M. Yang, H. Li, Construction of oxygen vacancy assisted Z-scheme BiO2-x/BiOBr heterojunction for LED light pollutants degradation and bacteria inactivation, J. Colloid Interface Sci. 600 (2021) 344–357, https://doi.org/10.1016/j.jcis.2021.04.143.

[46] C. Ouyang, X. Quan, C. Zhang, Y. Pan, X. Li, Z. Hong, M. Zhi, Direct Z-scheme ZnIn2S4@MoO3 heterojunction for efficient photodegradation of tetracycline hydrochloride under visible light irradiation, Chem. Eng. J. 424 (2021), 130510, https://doi.org/10.1016/j.cej.2021.130510.

[47] G. Yang, D. Chen, H. Ding, J. Feng, J.Z. Zhang, Y. Zhu, S. Hamid, D. W. Bahnemann, Well-designed 3D ZnIn2S4 nanosheets/TiO2 nanobelts as direct Z-scheme photocatalysts for CO2 photoreduction into renewable hydrocarbon fuel with high efficiency, Appl. Catal. B Environ. 219 (2017) 611–618, https://doi.org/10.1016/j.apcatb.2017.08.016.

[48] Z. Zhang, Z. Pan, Y. Guo, P. Keung, X. Zhou, R. Bai, In-situ growth of all-solid Z-scheme heterojunction photocatalyst of Bi7O9I3/g-C3N4 and high efficient degradation of antibiotic under visible light, Appl. Catal. B Environ. 261 (2020), 118212, https://doi.org/10.1016/j.apcatb.2019.118212.

[49] Z. Lin, Y. Zheng, F. Deng, X. Luo, J. Zou, P. Shao, S. Zhang, H. Tang, Target-directed design of dual-functional Z-scheme AgIn5S8/SnS2 heterojunction for Pb (II) capture and photocatalytic reduction of Cr(VI): Performance and mechanism insight, Sep. Purif. Technol. 277 (2021), 119430, https://doi.org/10.1016/j.seppur.2021.119430.

[50] J. Luo, X. Ning, L. Zhan, X. Zhou, Facile construction of a fascinating Z-scheme AgI/Zn3V2O8 photocatalyst for the photocatalytic degradation of tetracycline under visible light irradiation, Sep. Purif. Technol. 255 (2021), 117691, https://doi.org/10.1016/j.seppur.2020.117691.

[51] C. Liu, Y. Feng, Z. Han, Y. Sun, X. Wang, Q. Zhang, Z. Zou, Z-scheme N-doped K4Nb6O17/g-C3N4 heterojunction with superior visible-light-driven photocatalytic activity for organic pollutant removal and hydrogen production, Chinese, J. Catal. 42 (2021) 164–174, https://doi.org/10.1016/S1872-2067(20)63608-7.

[52] J. Li, H. Hao, Z. Zhu, Construction of g-C3N4-WO3-Bi2WO6 double Z-scheme system with enhanced photoelectrochemical performance, Mater. Lett. 168 (2016) 180–183, https://doi.org/10.1016/j.matlet.2016.01.058.

[53] M. Tang, Y. Ao, C. Wang, P. Wang, Rationally constructing of a novel dual Z-scheme composite photocatalyst with significantly enhanced performance for neonicotinoid degradation under visible light irradiation, Appl. Catal. B Environ. 270 (2020), 118918, https://doi.org/10.1016/j.apcatb.2020.118918.

[54] X. Yan, X. Yuan, J. Wang, Q. Wang, C. Zhou, D. Wang, H. Tang, J. Pan, X. Cheng, Construction of novel ternary dual Z-scheme Ag3VO4/C3N4/reduced TiO2 composite with excellent visible-light photodegradation activity, J. Mater. Chem. A. 34 (2019) 2024–2036, https://doi.org/10.1557/jmr.2019.164.

[55] Y. Wang, C. Zhu, G. Zuo, Y. Guo, W. Xiao, Y. Dai, J. Kong, X. Xu, Y. Zhou, A. Xie, C. Sun, Q. Xian, 0D/2D Co3O4/TiO2 Z-Scheme heterojunction for boosted photocatalytic degradation and mechanism investigation, Appl. Catal. B Environ. 278 (2020), 119298, https://doi.org/10.1016/j.apcatb.2020.119298.

[56] M. Ren, Y. Ao, P. Wang, C. Wang, Construction of silver/graphitic-C3N4/bismuth tantalate Z-scheme photocatalyst with enhanced visible-light-driven performance for sulfamethoxazole degradation, Chem. Eng. J. 378 (2019), 122122, https://doi.org/10.1016/j.cej.2019.122122.

[57] P. Chen, Q. Zhang, Y. Su, L. Shen, F. Wang, H. Liu, Y. Liu, Z. Cai, W. Lv, G. Liu, Accelerated photocatalytic degradation of diclofenac by a novel CQDs/BiOCOOH hybrid material under visible-light irradiation: Dechloridation, detoxicity, and a new superoxide radical model study, Chem. Eng. J. 332 (2018) 737–748.

[58] M.C. Weber, M. Guennou, N. Dix, D. Pesquera, G. Herranz, J. Fontcuberta, J. Kreisel, Multiple strain-induced phase transitions in LaNiO3 thin films, Phys. Rev. B. 94 (2016), 014118, https://doi.org/10.1103/PhysRevB.94.014118.

[59] S. Itapu, V. Borra, F. Mossayebi, A computational study on the variation of Bandgap due to native defects in non-stoichiometric NiO and Pd, Pt doping in stoichiometric NiO, Condens. Matter. 3 (2018) 46, https://doi.org/10.3390/condmat3040046.

[60] C. Feng, Y. Wang, Z. Lu, Q. Liang, Y. Zhang, Z. Li, S. Xu, Nanoflower Ni5P4 coupled with GCNQDs as Schottky junction photocatalyst for the efficient degradation of norfloxacin, Sep. Purif. Technol. 282 (2022), 120107, https://doi.org/10.1016/j.seppur.2021.120107.

[61] H. Deng, X. Fei, Y.i. Yang, J. Fan, J. Yu, B. Cheng, L. Zhang, S-scheme heterojunction based on p-type ZnMn2O4 and n-type ZnO with improved photocatalytic CO2 reduction activity, Chem. Eng. J. 409 (2021) 127377.

[62] Z. Wang, L. Jiang, K. Wang, Y. Li, G. Zhang, Novel AgI/BiSbO4 heterojunction for efficient photocatalytic degradation of organic pollutants under visible light: Interfacial electron transfer pathway, DFT calculation and degradation mechanism study, J. Hazard. Mater. 410 (2021), 124948, https://doi.org/10.1016/j.jhazmat.2020.124948.

[63] J. Low, J. Yu, C. Jiang, Design and fabrication of direct Z-scheme photocatalysts, in: Interface Sci. Technol., Elsevier Ltd., 2020: pp. 193–229. Doi: 10.1016/B978-0-08-102890-2.00006-3.

[64] K. Wenderich, G. Mul, Methods, Mechanism, and Applications of Photodeposition in Photocatalysis: A Review, Chem. Rev. 116 (2016) 14587–14619, https://doi.org/10.1021/acs.chemrev.6b00327.

[65] P. Zhang, Y. Li, Y. Zhang, R. Hou, X. Zhang, C. Xue, S. Wang, B. Zhu, N. Li, G. Shao, Photogenerated Electron Transfer Process in Heterojunctions: In Situ Irradiation XPS, Small Methods. 4 (2020) 2000214, https://doi.org/10.1002/smtd.202000214.

[66] W. Jo, T.S. Natarajan, Influence of TiO2 morphology on the photocatalytic efficiency of direct Z-scheme g-C3N4/TiO2 photocatalysts for isoniazid

degradation, Chem. Eng. J. 281 (2015) 549–565, https://doi.org/10.1016/j.cej.2015.06.120.
[67] Y. Wang, X. Shang, J. Shen, Z. Zhang, J.C.S. Wu, X. Fu, X. Wang, C. Li, D. Wang, J. Lin, Direct and indirect Z-scheme heterostructure-coupled photosystem enabling cooperation of CO2 reduction and H2O oxidation, Nat. Commun. 11 (2020) 3043, https://doi.org/10.1038/s41467-020-16742-3.
[68] P.J. Mafa, M.E. Malefane, A.O. Idris, D. Liu, J. Gui, B.B. Mamba, A.T. Kuvarega, Multi-elemental doped g-C3N4 with enhanced visible light photocatalytic Activity: Insight into naproxen Degradation, Kinetics, effect of Electrolytes, and mechanism, Sep. Purif. Technol. 282 (2022), 120089, https://doi.org/10.1016/j.seppur.2021.120089.
[69] Y. Xue, Z. Wu, X. He, Q. Li, X. Yang, L. Li, Hierarchical fabrication Z-scheme photocatalyst of BiVO4 (040)- Ag@CdS for enhanced photocatalytic properties under simulated sunlight irradiation, J. Colloid Interface Sci. 548 (2019) 293–302, https://doi.org/10.1016/j.jcis.2019.04.043.
[70] M.E. Aguirre, R. Zhou, A.J. Eugene, M.I. Guzman, M.A. Grela, Cu2O/TiO2 heterostructures for CO2 reduction through a direct Z-scheme: Protecting Cu2O from photocorrosion, Appl. Catal. B Environ. 217 (2017) 485–493, https://doi.org/10.1016/j.apcatb.2017.05.058.
[71] X. Wang, L. Liu, H. An, Y. Zhong, D. Wang, C. Tang, C. Hu, (Sr0.6Bi0.305)2Bi2O7 as a new visible-light-responsive photocatalyst: An experimental and theoretical study, Mater. Res. Bull. 118 (2019) 110484.
[72] R. Berera, R. Van Grondelle, J.T.M. Kennis, Ultrafast transient absorption spectroscopy: principles and application to photosynthetic systems, Photosynth. Res. 101 (2009) 105–118, https://doi.org/10.1007/s11120-009-9454-y.
[73] Y. Jiang, J. Liao, H. Chen, H.-H. Zhang, J. Li, X.-D. Wang, D. Kuang, All-Solid-State Z-Scheme a -Fe2O3/Amine- RGO/CsPbBr 3 Hybrids for Visible-Light-Driven Photocatalytic CO2 Reduction, Chem. 6 (2020) 766–780, https://doi.org/10.1016/j.chempr.2020.01.005.
[74] M.E. Malefane, U. Feleni, P.J. Mafa, A.T. Kuvarega, Fabrication of direct Z-scheme Co3O4/BiOI for ibuprofen and trimethoprim degradation under visible light irradiation, Appl. Surf. Sci. 514 (2020), 145940, https://doi.org/10.1016/j.apsusc.2020.145940.
[75] Q. Xie, W. He, S. Liu, C. Li, J. Zhang, P.K. Wong, Bifunctional S-scheme g-C3N4/Bi/BiVO4 hybrid photocatalysts toward toward artificial carbon cycling, Chinese, J. Catal. 41 (2020) 140–153, https://doi.org/10.1016/S1872-2067(19)63481-9.
[76] S. Qu, Y. Xiong, J. Zhang, Fabrication of GO/CDots/BiOI nanocomposites with enhanced photocatalytic 4-chlorophenol degradation and mechanism insight, Sep. Purif. Technol. 210 (2019) 382–389, https://doi.org/10.1016/j.seppur.2018.08.027.
[77] X. Gu, Q. Yan, Y. Wei, Y. Luo, Y. Sun, D. Zhao, F. Ji, X. Xu, Visible-light-responsive photocatalyst with a microsphere structure: preparation and photocatalytic performance of CQDs@BiOCl, J. Mater. Sci. Mater. Electron. 30 (2019) 16321–16336, https://doi.org/10.1007/s10854-019-02003-7.
[78] P. Yao, H. Liu, D. Wang, J. Chen, G. Li, T. An, Enhanced visible-light photocatalytic activity to volatile organic compounds degradation and deactivation resistance mechanism of titania confined inside a metal-organic framework, J. Colloid Interface Sci. 522 (2018) 174–182, https://doi.org/10.1016/j.jcis.2018.03.075.
[79] Y. Ao, K. Wang, P. Wang, C. Wang, J. Hou, Synthesis of novel 2D–2D p-n heterojunction BiOBr/La2Ti2O7 composite photocatalyst with enhanced photocatalytic performance under both UV and visible light irradiation, Appl. Catal. B Environ. 194 (2016) 157–168, https://doi.org/10.1016/j.apcatb.2016.04.050.
[80] Z. Dong, J. Pan, B. Wang, Z. Jiang, C. Zhao, J. Wang, C. Song, Y. Zheng, C. Cui, C. Li, The p-n-type Bi5O7I-modified porous C3N4 nano-heterojunction for enhanced visible light photocatalysis, J. Alloys Compd. 747 (2018) 788–795, https://doi.org/10.1016/j.jallcom.2018.03.112.
[81] X. Lu, W. Che, X. Hu, Y. Wang, A. Zhang, F. Deng, S. Luo, D.D. Dionysiou, The facile fabrication of novel visible-light-driven Z-scheme CuInS2/Bi2WO6 heterojunction with intimate interface contact by in situ hydrothermal growth strategy for extraordinary photocatalytic performance, Chem. Eng. J. 356 (2019) 819–829, https://doi.org/10.1016/j.cej.2018.09.087.
[82] T. Zhang, M. Maihemllti, K. Okitsu, D. Talifur, Y. Tursun, A. Abulizi, In situ self-assembled S-scheme BiOBr/pCN hybrid with enhanced photocatalytic activity for organic pollutant degradation and CO2 reduction, Appl. Surf. Sci. 556 (2021), 149828, https://doi.org/10.1016/j.apsusc.2021.149828.
[83] J. Wang, H. Yao, Z. Fan, L. Zhang, J. Wang, S. Zang, Z. Li, Indirect Z-Scheme BiOI/g-C3N4 Photocatalysts with Enhanced Photoreduction CO2 Activity under Visible Light Irradiation, ACS Appl. Mater. Interfaces. 8 (2016) 3765–3775, https://doi.org/10.1021/acsami.5b09901.
[84] J. Yan, C. Wang, H. Ma, Y. Li, Y. Liu, N. Suzuki, C. Terashima, A. Fujishima, X. Zhang, Photothermal synergic enhancement of direct Z-scheme behavior of Bi4TaO8Cl/W18O49 heterostructure for CO2 reduction, Appl. Catal. B Environ. 268 (2020), 118401, https://doi.org/10.1016/j.apcatb.2019.118401.
[85] V. Dutta, S. Sharma, P. Raizada, R. Kumar, V.K. Thakur, V.-H. Nguyen, A.M. Asiri, A.A.P. Khan, P. Singh, Recent progress on bismuth-based Z-scheme semiconductor photocatalysts for energy and environmental applications, J. Environ. Chem. Eng. 8 (6) (2020) 104505.
[86] J. Kang, C. Jin, Z. Li, M. Wang, Z. Chen, Y. Wang, Dual Z-scheme MoS2/g-C3N4/Bi24O31Cl10 ternary heterojunction photocatalysts for enhanced visible-light photodegradation of antibiotic, J. Alloys Compd. 825 (2020), 153975, https://doi.org/10.1016/j.jallcom.2020.153975.
[87] V. Khanal, N.O. Balayeva, C. Günnemann, Z. Mamiyev, R. Dillert, D. W. Bahnemann, V. (Ravi) Subramanian, Photocatalytic NOx removal using tantalum oxide nanoparticles: A benign pathway, Appl. Catal. B Environ. 291 (2021), 119974, https://doi.org/10.1016/j.apcatb.2021.119974.
[88] X. Xu, L. Meng, Y. Dai, M. Zhang, C. Sun, S. Yang, H. He, S. Wang, H. Li, Bi spheres SPR-coupled Cu2O/Bi2MoO6 with hollow spheres forming Z- scheme Cu2O/Bi/Bi2MoO6 heterostructure for simultaneous photocatalytic decontamination of sulfadiazine and Ni (II), J. Hazard. Mater. 381 (2020), 120953, https://doi.org/10.1016/j.jhazmat.2019.120953.
[89] M. Ebihara, T. Ikeda, S. Okunaka, H. Tokudome, K. Domen, K. Katayama, Charge carrier mapping for Z-scheme photocatalytic water-splitting sheet via categorization of microscopic time-resolved image sequences, Nat. Commun. 12 (2021) 3716, https://doi.org/10.1038/s41467-021-24061-4.
[90] Y. Guo, Y. Ao, P. Wang, C. Wang, Mediator-free direct dual-Z-scheme Bi2S3/BiVO4/MgIn2S4 composite photocatalysts with enhanced visible-light-driven performance towards carbamazepine degradation, Appl. Catal. B Environ. 254 (2019) 479–490, https://doi.org/10.1016/j.apcatb.2019.04.031.
[91] Y. Yuan, R. Guo, L. Hong, X. Ji, Z. Lin, Z. Li, W. Pan, A review of metal oxide-based Z-scheme heterojunction photocatalysts: actualities and developments, Mater. Today Energy. 21 (2021), 100829, https://doi.org/10.1016/j.mtener.2021.100829.
[92] K. Liu, H. Zhang, Y. Muhammad, T. Fu, R. Tang, Z. Tong, Y. Wang, Fabrication of n-n isotype BiOBr-Bi2WO6 heterojunctions by inserting Bi2WO6 nanosheets onto BiOBr microsphere for the superior photocatalytic degradation of Ciprofloxacin and tetracycline, Sep. Purif. Technol. 274 (2021), 118992, https://doi.org/10.1016/j.seppur.2021.118992.
[93] Z. Wang, B. Cheng, L. Zhang, J. Yu, Y. Li, S. Wageh, A.A. Al, S - Scheme 2D / 2D Bi 2 MoO 6 / BiOI van der Waals heterojunction for CO 2 photoreduction, Chinese, J. Catal. 43 (2022) 1657–1666, https://doi.org/10.1016/S1872-2067(21)64010-X.
[94] A. Kumar, G. Sharma, A. Kumari, C. Guo, M. Naushad, D.-V.-N. Vo, J. Iqbal, F. J. Stadler, Construction of dual Z-scheme g-C3N4/Bi4Ti3O12/Bi4O5I2 heterojunction for visible and solar powered coupled photocatalytic antibiotic degradation and hydrogen production: boosting via I−/I−3 and Bi3+/Bi5+ redox mediators, Appl. Catal. B Environ. 284 (2021), 119808, https://doi.org/10.1016/j.apcatb.2020.119808.
[95] J. Zhang, Z. Zhu, J. Jiang, H. Li, Synthesis of Novel Ternary Dual Z-scheme AgBr/LaNiO3/g-C3N4 Composite with Boosted Visible-Light Photodegradation of Norfloxacin, Molecules. 25 (2020) 3706, https://doi.org/10.3390/molecules25163706.
[96] X. Zhou, Y. Chen, C. Li, L. Zhang, X. Zhang, X. Ning, L. Zhan, J. Luo, Construction of LaNiO3 nanoparticles modified g-C3N4 nanosheets for enhancing visible light photocatalytic activity towards tetracycline degradation, Sep. Purif. Technol. 211 (2019) 179–188, https://doi.org/10.1016/j.seppur.2018.09.075.
[97] S. Luo, R. Liu, X. Zhang, R. Chen, M. Yan, K. Huang, J. Sun, R. Wang, J. Wang, Mechanism investigation for ultra-efficient photocatalytic water disinfection based on rational design of indirect Z-scheme heterojunction black phosphorus QDs/Cu2O nanoparticles, J. Hazard. Mater. 424 (2022), 127281, https://doi.org/10.1016/j.jhazmat.2021.127281.
[98] Y. Qu, X. Li, H. Zhang, R. Huang, W. Qi, R. Su, Z. He, Controllable synthesis of a sponge-like Z-scheme N, S-CQDs/Bi2MoO6@TiO2 film with enhanced photocatalytic and antimicrobial activity under visible/NIR light irradiation, J. Hazard. Mater. 429 (2022), 128310, https://doi.org/10.1016/j.jhazmat.2022.128310.
[99] C. Piao, L. Chen, Z. Liu, J. Tang, Y. Liu, Y. Lin, D. Fang, J. Wang, Construction of solar light-driven dual Z-scheme Bi2MoO6/Bi2WO6\AgI\Ag photocatalyst for enhanced simultaneous degradation and conversion of nitrogenous organic pollutants, Sep. Purif. Technol. 274 (2021), 119140, https://doi.org/10.1016/j.seppur.2021.119140.
[100] C. Chen, Z. Li, Y. Guo, L. Ling, Y. Zheng, L. Ren, M. Wu, A Z-scheme iron-based hollow microsphere with enhanced photocatalytic performance for tetracycline degradation, J. Mater. Res. 36 (2021) 1600–1613, https://doi.org/10.1557/s43578-021-00208-3.
[101] V.D. Dang, J. Adorna Jr, T. Annadurai, T.A.N. Bui, H.L. Tran, L.-Y. Lin, R.-A. Doong, Indirect Z-scheme nitrogen-doped carbon dot decorated Bi2MoO6/g-C3N4 photocatalyst for enhanced visible-light-driven degradation of ciprofloxacin, Chem. Eng. J. 422 (2021), 130103, https://doi.org/10.1016/j.cej.2021.130103.
[102] P.J. Mafa, M.E. Malefane, A.O. Idris, B.B. Mamba, D. Liu, J. Gui, A.T. Kuvarega, Cobalt oxide/copper bismuth oxide/samarium vanadate (Co3O4/CuBi2O4/SmVO4) dual Z-scheme heterostructured photocatalyst with high charge-transfer efficiency: Enhanced carbamazepine degradation under visible light irradiation, J. Colloid Interface Sci. 603 (2021) 666–684, https://doi.org/10.1016/j.jcis.2021.06.146.
[103] B. Shao, X. Liu, Z. Liu, G. Zeng, Q. Liang, C. Liang, Y. Cheng, W. Zhang, Y. Liu, S. Gong, A novel double Z-scheme photocatalyst Ag3PO4/Bi2S3/Bi2O3 with enhanced visible-light photocatalytic performance for antibiotic degradation, Chem. Eng. J. 368 (2019) 730–745.
[104] A. Khan, M. Danish, U. Alam, S. Zafar, M. Muneer, Facile Synthesis of a Z-Scheme ZnIn2S4/MoO3 Heterojunction with enhanced photocatalytic activity under visible light irradiation, ACS Omega. 5 (2020) 8188–8199, https://doi.org/10.1021/acsomega.0c00446.
[105] D. Xia, W. Wang, R. Yin, Z. Jiang, T. An, G. Li, H. Zhao, P.K. Wong, Enhanced photocatalytic inactivation of Escherichia coli by a novel Z-scheme g-C3N4/m-Bi2O4 hybrid photocatalyst under visible light: The role of reactive oxygen species, Appl. Catal. B Environ. 214 (2017) 23–33, https://doi.org/10.1016/j.apcatb.2017.05.035.

[106] C. Zhang, M. Zhang, Y. Li, D. Shuai, Visible-light-driven photocatalytic disinfection of human adenovirus by a novel heterostructure of oxygen-doped graphitic carbon nitride and hydrothermal carbonation carbon, Appl. Catal. B Environ. 248 (2019) 11–21, https://doi.org/10.1016/j.apcatb.2019.02.009.
[107] H. Che, G. Che, E. Jiang, C. Liu, H. Dong, C. Li, A novel Z-Scheme CdS/Bi3O4Cl heterostructure for photocatalytic degradation of antibiotics: Mineralization activity, degradation pathways and mechanism insight, J. Taiwan Inst. Chem. Eng. 91 (2018) 224–234, https://doi.org/10.1016/j.jtice.2018.05.004.
[108] P. Teng, Z. Li, S. Gao, K. Li, M. Bowkett, N. Copner, Z. Liu, X. Yang, Fabrication of one-dimensional Bi2WO6/CuBi2O4 heterojunction nanofiber and its photocatalytic degradation property, Opt. Mater. (Amst). 121 (2021), 111508, https://doi.org/10.1016/j.optmat.2021.111508.
[109] B.O. Orimolade, A.O. Idris, U. Feleni, B. Mamba, Recent advances in degradation of pharmaceuticals using Bi2WO6 mediated photocatalysis – A comprehensive review, Environ. Pollut. 289 (2021), 117891, https://doi.org/10.1016/j.envpol.2021.117891.
[110] X. Zhang, Y. Zhang, X. Jia, N. Zhang, R. Xia, X. Zhang, Z. Wang, M. Yu, In situ fabrication of a novel S-scheme heterojunction photocatalyts Bi2O3/P-C3N4 to enhance levofloxacin removal from water, Sep. Purif. Technol. 268 (2021), 118691, https://doi.org/10.1016/j.seppur.2021.118691.
[111] M. Wang, H. Yu, P. Wang, Z. Chi, Z. Zhang, B. Dong, H. Dong, K. Yu, H. Yu, Promoted photocatalytic degradation and detoxication performance for norfloxacin on Z-scheme phosphate-doped BiVO4/graphene quantum dots/ P-doped g-C3N4, Sep. Purif. Technol. 274 (2021), 118692, https://doi.org/10.1016/j.seppur.2021.118692.
[112] S.L. Prabavathi, K. Saravanakumar, C.M. Park, V. Muthuraj, Photocatalytic degradation of levofloxacin by a novel Sm6WO12/g-C3N4 heterojunction: Performance, mechanism and degradation pathways, Sep. Purif. Technol. 257 (2021), 117985, https://doi.org/10.1016/j.seppur.2020.117985.
[113] K. Wu, Z. Qin, X. Zhang, R. Guo, X. Ren, X. Pu, Z-scheme BiOCl/Bi–Bi2O3 heterojunction with oxygen vacancy for excellent degradation performance of antibiotics and dyes, J. Mater. Sci. 55 (2020) 4017–4029, https://doi.org/10.1007/s10853-019-04300-2.
[114] X. Ren, X. Zhang, R. Guo, X. Li, Y. Peng, X. Zhao, X. Pu, Hollow mesoporous g-C3N4/Ag2CrO4 photocatalysis with direct Z-scheme: Excellent degradation performance for antibiotics and dyes, Sep. Purif. Technol. 270 (2021) 118797.
[115] Y. Wang, L. Ding, C. Liu, Y. Lu, Q. Wu, C. Wang, Q. Hu, 0D/2D/2D ZnFe2O4/Bi2O2CO3/BiOBr double Z-scheme heterojunctions for the removal of tetracycline antibiotics by permonosulfate activation: Photocatalytic and non-photocatalytic mechanisms, radical and non-radical pathways, Sep. Purif. Technol. 283 (2022), 120164, https://doi.org/10.1016/j.seppur.2021.120164.
[116] X.-J. Wen, Qian-Lu, X.-X. Lv, J. Sun, J. Guo, Z.-H. Fei, C.-G. Niu, Photocatalytic degradation of sulfamethazine using a direct Z-Scheme AgI/Bi4V2O11 photocatalyst: Mineralization activity, degradation pathways and promoted charge separation mechanism, J. Hazard. Mater. 385 (2020) 121508.
[117] A. Kumar, G. Sharma, M. Naushad, Z.A. Alothman, P. Dhiman, Environmental Pollution Remediation via Photocatalytic Degradation of Sulfamethoxazole from Waste Water Using Sustainable Ag2S/Bi2S3/g-C3N4 Nano-Hybrids, Earth Syst. Environ. 26 (2022) 141–156, https://doi.org/10.1007/s41748-021-00223-8.
[118] WHO, 18th WHO Model List of Essential Medicines, 18 th edit, London, UK, 2013. http://www.who.int/medicines/publications/essentialmedicines/en/index.html.
[119] X. Xie, S. Li, K. Qi, Z. Wang, Photoinduced synthesis of green photocatalyst Fe3O4/BiOBr/CQDs derived from corncob biomass for carbamazepine degradation: The role of selectively more CQDs decoration and Z-scheme structure, Chem. Eng. J. 420 (2021), 129705, https://doi.org/10.1016/j.cej.2021.129705.
[120] M. Scheurell, S. Franke, R.M. Shah, H. Hühnerfuss, Occurrence of diclofenac and its metabolites in surface water and effluent samples from Karachi, Pakistan, Chemosphere. 77 (2009) 870–876, https://doi.org/10.1016/j.chemosphere.2009.07.066.
[121] W. Li, R. Yu, M. Li, N. Guo, H. Yu, Y. Yu, Photocatalytical degradation of diclofenac by Ag-BiOI-rGO: Kinetics, mechanisms and pathways, Chemosphere. 218 (2019) 966–973, https://doi.org/10.1016/j.chemosphere.2018.11.185.
[122] A. Ivanets, V. Prozorovich, M. Roshchina, I. Grigoraviciute-puroniene, A. Zarkov, A. Kareiva, Z. Wang, V. Srivastava, M. Sillanpää, Heterogeneous Fenton Oxidation Using Magnesium Ferrite Nanoparticles for Ibuprofen Removal from Wastewater : Optimization and Kinetics Studies, J. Nanomater. 2020 (2020) 8159628, https://doi.org/10.1155/2020/8159628.
[123] S. Wu, X. Yu, J. Zhang, Y. Zhang, Y. Zhu, M. Zhu, Construction of BiOCl/CuBi2O4 S-scheme heterojunction with oxygen vacancy for enhanced photocatalytic diclofenac degradation and nitric oxide removal, Chem. Eng. J. 411 (2021), 128555, https://doi.org/10.1016/j.cej.2021.128555.
[124] P.J. Mafa, U.S. Swana, D. Liu, J. Gui, B.B. Mamba, A.T. Kuvarega, Synthesis of Bi5O7I-MoO3 Photocatalyst via Simultaneous Calcination of BiOI and MoS2 for Visible Light Degradation of Ibuprofen, Colloids Surfaces A Physicochem. Eng. Asp. 612 (2021), 126004, https://doi.org/10.1016/j.colsurfa.2020.126004.
[125] Q. Wei, S. Xiong, W. Li, C. Jin, Y. Chen, L. Hou, Z. Wu, Z. Pan, Q. He, Y. Wang, D. Tang, Double Z-scheme system of α-SnWO4/UiO-66(NH2)/g-C3N4 ternary heterojunction with enhanced photocatalytic performance for ibuprofen degradation and H2 evolution, J. Alloys Compd. 885 (2021), 160984, https://doi.org/10.1016/j.jallcom.2021.160984.
[126] C. Xing, G. Yu, T. Chen, S. Liu, Q. Sun, Q. Liu, Y. Hu, H. Liu, X. Li, Perylenetetracarboxylic diimide covalently bonded with mesoporous g-C3N4 to construct direct Z-scheme heterojunctions for efficient photocatalytic oxidative coupling of amines, Appl. Catal. B Environ. 298 (2021), 120534, https://doi.org/10.1016/j.apcatb.2021.120534.
[127] X. Liu, J. Zhou, D. Liu, L. Li, W. Liu, S. Liu, C. Feng, Construction of Z-scheme CuFe2O4/MnO2 photocatalyst and activating peroxymonosulfate for phenol degradation: Synergistic effect, degradation pathways, and mechanism, Environ. Res. 200 (2021), 111736, https://doi.org/10.1016/j.envres.2021.111736.
[128] G. Mamba, P.J. Mafa, V. Muthuraj, A. Mashayekh-Salehi, S. Royer, T.I. T. Nkambule, S. Rtimi, Heterogeneous advanced oxidation processes over stoichiometric ABO3 perovskite nanostructures, Mater. Today Nano. 18 (2022), 100184, https://doi.org/10.1016/j.mtnano.2022.100184.
[129] Y. Peng, H. Tang, B. Yao, X. Gao, X. Yang, Y. Zhou, Activation of peroxymonosulfate (PMS) by spinel ferrite and their composites in degradation of organic pollutants: A Review, Chem. Eng. J. 414 (2021), 128800, https://doi.org/10.1016/j.cej.2021.128800.
[130] W. Liu, Q. Kang, L. Wang, L. Wen, Z. Li, Facile synthesis of Z-scheme g-C3N4@MIL-100 (Fe) and the efficient photocatalytic degradation on doxycycline and disinfection by-products by coupling with persulfate: Mechanism and pathway, Colloids Surfaces A Physicochem. Eng. Asp. 635 (2022), 128057, https://doi.org/10.1016/j.colsurfa.2021.128057.
[131] C. Liu, S. Mao, M. Shi, F. Wang, M. Xia, Q. Chen, X. Ju, Peroxymonosulfate activation through 2D/2D Z-scheme CoAl-LDH/BiOBr photocatalyst under visible light for ciprofloxacin degradation, J. Hazard. Mater. 420 (2021) 126613.
[132] Q. Ji, X. Cheng, X. Kong, D. Sun, Y. Wu, Z. Xu, Y. Liu, X. Duan, H. He, S. Li, L. Zhang, S. Yang, Visible-light activation of persulfate ions by Z-scheme perylene diimide/MIL-101(Cr) heterojunction photocatalyst towards efficient degradation of iohexol, Chem. Eng. J. 435 (2022), 134947, https://doi.org/10.1016/j.cej.2022.134947.
[133] M. Ding, W. Ao, H. Xu, W. Chen, L. Tao, Z. Shen, H. Liu, C. Lu, Z. Xie, Facile construction of dual heterojunction CoO@TiO2/MXene hybrid with efficient and stable catalytic activity for phenol degradation with peroxymonosulfate under visible light irradiation, J. Hazard. Mater. 420 (2021) 126686.
[134] S. Wacławek, H.V. Lutze, K. Grübel, V.V.T. Padil, M. Černík, D.D. Dionysiou, Chemistry of persulfates in water and wastewater treatment: A review, Chem. Eng. J. 330 (2017) 44–62, https://doi.org/10.1016/j.cej.2017.07.132.
[135] V. Hasija, V.H. Nguyen, A. Kumar, P. Raizada, V. Krishnan, A.A.P. Khan, P. Singh, E. Lichtfouse, C. Wang, P. Thi Huong, Advanced activation of persulfate by polymeric g-C3N4 based photocatalysts for environmental remediation: A review, J. Hazard. Mater. 413 (2021), 125324, https://doi.org/10.1016/j.jhazmat.2021.125324.
[136] X. Yu, W. Qin, X. Yuan, L. Sun, F. Pan, D. Xia, Synergistic mechanism and degradation kinetics for atenolol elimination via integrated UV/ozone/peroxymonosulfate process, J. Hazard. Mater. 407 (2021), 124393, https://doi.org/10.1016/j.jhazmat.2020.124393.
[137] J. Lyu, M. Ge, Z. Hu, C. Guo, One-pot synthesis of magnetic CuO/Fe2O3/CuFe2O4 nanocomposite to activate persulfate for levofloxacin removal: Investigation of efficiency, mechanism and degradation route, Chem. Eng. J. 389 (2020), 124456, https://doi.org/10.1016/j.cej.2020.124456.
[138] Y. Lv, Y. Liu, J. Wei, M. Li, D. Xu, B. Lai, Bisphenol S degradation by visible light assisted peroxymonosulfate process based on BiOI/B4C photocatalysts with Z-scheme heterojunction, Chem. Eng. J. 417 (2021), 129188, https://doi.org/10.1016/j.cej.2021.129188.
[139] S. Dhaka, R. Kumar, S. Lee, M.B. Kurade, B. Jeon, Degradation of ethyl paraben in aqueous medium using advanced oxidation processes : Ef fi ciency evaluation of UV-C supported oxidants, J. Clean. Prod. 180 (2018) 505–513, https://doi.org/10.1016/j.jclepro.2018.01.197.
[140] G. Zhang, T. Dai, Y. Meng, L. Zhang, C. Yang, G. Pan, Z. Ni, S. Xia, Z-Scheme heterojunction ZnO-Au-ZnAl2O4: Bridge-type hot carrier transfer and reaction kinetics in the photodegradation of catechol, Appl. Surf. Sci. 532 (2020), 147456, https://doi.org/10.1016/j.apsusc.2020.147456.
[141] Z. Wang, H. Wang, Z. Zeng, G. Zeng, P. Xu, R. Xiao, D. Huang, X. Chen, L. He, C. Zhou, Y. Yang, Z. Wang, W. Wang, W. Xiong, Metal-organic frameworks derived Bi2O2CO3/porous carbon nitride: A nanosized Z-scheme systems with enhanced photocatalytic activity, Appl. Catal. B Environ. 267 (2020), 118700, https://doi.org/10.1016/j.apcatb.2020.118700.
[142] Y. Wu, S. Mao, C. Liu, F. Pei, F. Wang, Q. Hao, M. Xia, W. Lei, Enhanced degradation of chloramphenicol through peroxymonosulfate and visible light over Z-scheme Photocatalysts: Synergetic performance and mechanism insights, J. Colloid Interface Sci. 608 (2022) 322–333, https://doi.org/10.1016/j.jcis.2021.09.197.
[143] C. Yang, G. Zhang, Y. Meng, G. Pan, Z. Ni, S. Xia, Direct Z-scheme CeO2@LDH core–shell heterostructure for photodegradation of Rhodamine B by synergistic persulfate activation, J. Hazard. Mater. 408 (2021) 124908.
[144] S.W. Lv, J.M. Liu, N. Zhao, C.Y. Li, F.E. Yang, Z.H. Wang, S. Wang, MOF-derived CoFe2O4/Fe2O3 embedded in g-C3N4 as high-efficient Z-scheme photocatalysts for enhanced degradation of emerging organic pollutants in the presence of persulfate, Sep. Purif. Technol. 253 (2020), 117413, https://doi.org/10.1016/j.seppur.2020.117413.
[145] D. Venieri, I. Gounaki, V. Binas, A. Zachopoulos, G. Kiriakidis, D. Mantzavinos, Inactivation of MS2 coliphage in sewage by solar photocatalysis using metal-doped TiO2, Appl. Catal. B Environ. 178 (2015) 54–64, https://doi.org/10.1016/j.apcatb.2014.10.052.
[146] J.C. Sjogren, R.A. Sierka, Inactivation of Phage MS2 by Iron-Aided Titanium Dioxide Photocatalysis, Appl. Environ. Microbiol. 60 (1994) 344–347, https://doi.org/10.1128/aem.60.1.344-347.1994.
[147] A. Habibi-yangjeh, S. Asadzadeh-khaneghah, S. Feizpoor, A. Rouhi, Review on heterogeneous photocatalytic disinfection of waterborne, airborne, and foodborne viruses: Can we win against pathogenic viruses? J. Colloid Interface Sci. 580 (2020) 503–514, https://doi.org/10.1016/j.jcis.2020.07.047.

[148] Y. Zhou, L. Zhou, Y. Zhou, M. Xing, J. Zhang, Z-scheme photo-Fenton system for efficiency synchronous oxidation of organic contaminants and reduction of metal ions, Appl. Catal. B Environ. 279 (2020), 119365, https://doi.org/10.1016/j.apcatb.2020.119365.
[149] V. Hasija, S. Patial, P. Singh, V. Nguyen, Q. Van Le, V.K. Thakur, C.M. Hussain, R. Selvasembian, C. Huang, S. Thakur, P. Raizada, Photocatalytic Inactivation of Viruses Using Graphitic Carbon and Mechanism, Catalysts. 11 (2021) 1448, https://doi.org/10.3390/catal11121448.
[150] Y. Xiang, Q. Zhou, Z. Li, Z. Cui, X. Liu, Y. Liang, S. Zhu, Y. Zheng, K.W.K. Yeung, S. Wu, A Z-scheme heterojunction of ZnO/CDots/C3N4 for strengthened photoresponsive bacteria-killing and acceleration of wound healing, J. Mater. Sci. Technol. 57 (2020) 1–11, https://doi.org/10.1016/j.jmst.2020.05.016.
[151] T. Kato, H. Tohma, O. Miki, T. Shibata, M. Tamura, Degradation of Norovirus in Sewage Treatment Water by Photocatalytic Ultraviolet Disinfection, Nippon Steel Tech. Rep. UDC 614 (48) (2005) 41–44.
[152] S. Rtimi, J. Kiwi, Update on Interfacial Charge Transfer (IFTC) Processes on Films Inactivating Viruses/Bacteria under Visible Light: Mechanistic Considerations and Critical Issues, Catalysts. 11 (2021) 201, https://doi.org/10.3390/catal11020201.
[153] C. Zhang, Y. Li, D. Shuai, Y. Shen, D. Wang, Progress and challenges in photocatalytic disinfection of waterborne Viruses: A review to fill current knowledge gaps, Chem. Eng. J. 355 (2019) 399–415, https://doi.org/10.1016/j.cej.2018.08.158.
[154] R. Cheng, L. Shen, J. Yu, S. Xiang, X. Zheng, Photocatalytic Inactivation of Bacteriophage f2 with Ag3PO4/g-C3N4 Composite under Visible Light Irradiation: Performance and Mechanism, Catalysts. 8 (2018) 406, https://doi.org/10.3390/catal8100406.
[155] F. Chang, J. Zheng, F. Wu, X. Wang, B. Deng, Binary composites WO3/g-C3N4 in porous morphology: Facile construction, characterization, and reinforced visible light photocatalytic activity, Colloids Surfaces A Physicochem. Eng. Asp. 563 (2019) 11–21, https://doi.org/10.1016/j.colsurfa.2018.11.058.
[156] W. Shi, X. Guo, C. Cui, K. Jiang, Z. Li, L. Qu, J.-C. Wang, Controllable synthesis of Cu2O decorated WO3 nanosheets with dominant (001) facets for photocatalytic CO2 reduction under visible-light irradiation, Appl. Catal. B Environ. 243 (2019) 236–242, https://doi.org/10.1016/j.apcatb.2018.09.076.
[157] J. Liu, L. Huang, Y. Li, L. Yang, C. Wang, J. Liu, Y. Song, M. Yang, H. Li, Construction of oxygen vacancy assisted Z-scheme BiO2Ax/BiOBr heterojunction for LED light pollutants degradation and bacteria inactivation, J. Colloid Interface Sci. 600 (2021) 344–357, https://doi.org/10.1016/j.jcis.2021.04.143.
[158] P.K. Prajapati, D. Garg, A. Malik, D. Kumar, V. Amoli, S.L. Jain, A novel ternary metal oxide cascade Z-scheme heterojunction for efficient CO2 photoconversion without a co-catalyst, J. Environ. Chem. Eng. 10 (4) (2022) 108147.
[159] G. Fan, R. Ning, Z. Yan, J. Luo, B. Du, J. Zhan, L. Liu, J. Zhang, Double photoelectron-transfer mechanism in Ag−AgCl/WO3/g-C3N4 photocatalyst with enhanced visible-light photocatalytic activity for trimethoprim degradation, J. Hazard. Mater. 403 (2021), 123964, https://doi.org/10.1016/j.jhazmat.2020.123964.
[160] J. Fu, Q. Xu, J. Low, C. Jiang, J. Yu, Ultrathin 2D/2D WO3/g-C3N4 step-scheme H2-production photocatalyst, Appl. Catal. B Environ. 243 (2019) 556–565, https://doi.org/10.1016/j.apcatb.2018.11.011.
[161] Y. Xia, Z. He, J. Su, B. Tang, Y. Liu, Enhanced photocatalytic performance of Z-scheme - Cu2O/Bi5O7I nanocomposites, J. Mater. Sci. Mater. Electron. 29 (2018) 15271–15281, https://doi.org/10.1007/s10854-018-9669-9.
[162] H. Yang, R. Cao, P. Sun, J. Yin, S. Zhang, X. Xu, Constructing electrostatic self-assembled 2D/2D ultra-thin ZnIn2S4/protonated g-C3N4 heterojunctions for excellent photocatalytic performance under visible light, Appl. Catal. B Environ. 256 (2019), 117862, https://doi.org/10.1016/j.apcatb.2019.117862.
[163] D. Wang, Y. Ao, P. Wang, Effective inactivation of Microcystis aeruginosa by a novel Z -scheme composite photocatalyst under visible light irradiation, Sci. Total Environ. 746 (2020), 141149, https://doi.org/10.1016/j.scitotenv.2020.141149.
[164] W. Xu, W. Tian, L. Meng, F. Cao, L. Li, Interfacial Chemical Bond-Modulated Z-scheme Charge Transfer for Efficient Photoelectrochemical Water Splitting, Adv. Energy Mater. 11 (2021) 2003500. https://doi.org/10.1oo2/aenm.202003500.
[165] M.G. Alalm, R. Djellabi, D. Meroni, C. Pirola, C.L. Bianchi, D.C. Boffito, Toward Scaling-Up Photocatalytic Process for Multiphase Environmental Applications, Catayst. 11 (2021) 562, https://doi.org/10.3390/catal11050562.
[166] Y. Lai, D. Lee, Pollutant degradation with mediator Z-scheme heterojunction photocatalyst in water: A review, Chemosphere. 282 (2021), 131059, https://doi.org/10.1016/j.chemosphere.2021.131059.
[167] R.B. Chandran, S. Breen, Y. Shao, S. Ardo, A.Z. Weber, Evaluating particle-suspension reactor designs for Z-scheme solar water splitting via transport and kinetic modeling, Energy Environ. Sci. 11 (2018) 115–135, https://doi.org/10.1039/C7EE01360D.
[168] W. Su, D.W. Ayele, H. Chen, C. Pan, V. Ochie, K. Chiang, J. Rick, B.-J. Hwang, A wireless and redox mediator-free Z-scheme twin reactor for the separate evolution of hydrogen and oxygen, Mater. Today Energy. 12 (2019) 208–214, https://doi.org/10.1016/j.mtener.2019.01.009.
[169] J. Mo, Y. Zhang, Q. Xu, J.J. Lamson, R. Zhao, Photocatalytic purification of volatile organic compounds in indoor air: A literature review, Atmos. Environ. 43 (2009) 2229–2246, https://doi.org/10.1016/j.atmosenv.2009.01.034.